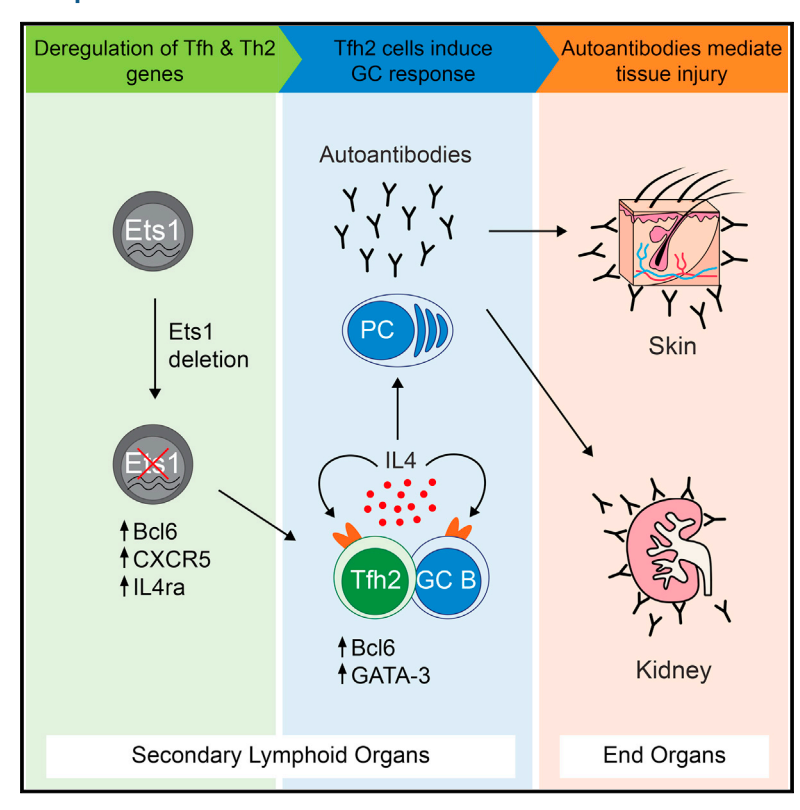
# **Immunity**

# The Transcription Factor Ets1 Suppresses T Follicular Helper Type 2 Cell Differentiation to Halt the Onset of Systemic Lupus Erythematosus

# **Graphical Abstract**



# **Authors**

Chan Johng Kim, Choong-Gu Lee, Ju-Yang Jung, ..., Dipayan Rudra, Chang-Hee Suh, Sin-Hyeog Im

# Correspondence

iimsh@postech.ac.kr

# In Brief

Single-nucleotide polymorphisms in *ETS1* are associated with systemic lupus erythematosus (SLE). Kim et al. show that *Ets1* deletion in T cells, but not B cells or DCs, result in SLE-like humoral autoimmunity, which was due to the expansion of GATA-3\*Bcl6\* Tfh2 cells and could be alleviated by neutralizing IL-4. Tfh2 frequencies in SLE patients correlate with disease parameters, suggesting therapeutic relevance for IL-4 blockade.

# **Highlights**

- Ets1 deletion in T cells, but not B cells or DCs, induces SLElike autoimmunity in mice
- GATA-3\*Bcl6\*IL4\* Tfh2 cells drive autoimmunity in Ets1<sup>ΔCD4</sup> mice
- IL-4 neutralization suppresses Tfh2 cells and SLE progression
- Low ETS1 correlates with high Tfh:Tfh2 cell frequencies in SLE patients







# The Transcription Factor Ets1 Suppresses T Follicular Helper Type 2 Cell Differentiation to Halt the Onset of Systemic Lupus Erythematosus

Chan Johng Kim,<sup>1,2</sup> Choong-Gu Lee,<sup>1</sup> Ju-Yang Jung,<sup>3</sup> Ambarnil Ghosh,<sup>1</sup> Syed Nurul Hasan,<sup>1,2</sup> Sung-Min Hwang,<sup>1,2</sup> Hyeji Kang,<sup>1</sup> Changhon Lee,<sup>1,2</sup> Gi-Cheon Kim,<sup>1</sup> Dipayan Rudra,<sup>1</sup> Chang-Hee Suh,<sup>3</sup> and Sin-Hyeog Im<sup>1,2,4,\*</sup>

<sup>1</sup>Academy of Immunology and Microbiology, Institute for Basic Science, Pohang, Gyeongbuk 37673, Republic of Korea

#### **SUMMARY**

Single-nucleotide polymorphisms in ETS1 are associated with systemic lupus erythematosus (SLE). Ets1<sup>-/-</sup> mice develop SLE-like symptoms, suggesting that dysregulation of this transcription factor is important to the onset or progression of SLE. We used conditional deletion approaches to examine the impact of Ets1 expression in different immune cell types. Ets1 deletion on CD4+ T cells, but not B cells or dendritic cells, resulted in the SLE autoimmunity, and this was associated with the spontaneous expansion of T follicular helper type 2 (Tfh2) cells. Ets1<sup>-/-</sup> Tfh2 cells exhibited increased expression of GATA-3 and interleukin-4 (IL-4), which induced IgE isotype switching in B cells. Neutralization of IL-4 reduced Tfh2 cell frequencies and ameliorated disease parameters. Mechanistically, Ets1 suppressed signature Tfh and Th2 cell genes, including Cxcr5, Bcl6, and Il4ra, thus curbing the terminal Tfh2 cell differentiation process. Tfh2 cell frequencies in SLE patients correlated with disease parameters, providing evidence for the relevance of these findings to human disease.

# INTRODUCTION

Systemic lupus erythematosus (SLE) is an antibody-mediated autoimmune disease where multiple organs come under attack from the host's immune system, causing significant organ damage (Kaul et al., 2016). Plasma cells (PCs) are the main producers of these pathogenic antibodies, whereas type 1 interferons (IFN-I), mainly secreted by plasmacytoid dendritic cells (pDCs), amplify this process by enhancing B cell proliferation and differentiation (Banchereau and Pascual, 2006). Consistently, SLE patients display higher numbers of PC precursors and memory B cells and a higher serum concentration of IFN-I than healthy in-

dividuals (Crow, 2014; Dörner et al., 2009). Thus, immunotherapeutic strategies for the treatment of SLE so far have been focused on targeting B cells and IFN-I signaling. These clinical trials, however, rarely reach the points of their expected effectiveness, suggesting that alternative therapeutic strategies should be considered (Mok and Shoenfeld, 2016). Along these lines, the role of T cells in augmenting humoral autoimmunity has recently been highlighted. T follicular helper (Tfh) cells induce germinal center responses, leading to autoantibody production, whereas T helper 1 (Th1) and T helper 17 (Th17) cells contribute to immunoglobulin isotype switching and lupus nephritis (Blanco et al., 2016; Martin et al., 2014; Richards et al., 2001).

SLE development is influenced by genetic alterations of SLEassociated genes. Genome-wide association studies (GWASs) have identified over 60 SLE-linked risk loci, including ETS1, STAT4, TNFSF4, and WDFY4 (Sun et al., 2016). ETS1 shows the third highest discovery rate in Asian SLE patients, and Ets1<sup>-/-</sup> mice spontaneously develop SLE-like disease (Sun et al., 2016; Wang et al., 2005; Yang et al., 2010), suggesting a central role for Ets1 function in SLE. Ets1 is a transcription factor that is highly expressed in B cells, thymocytes, T cells, and pDCs but is also expressed at lower amounts in germinal center B (GC B) cells, PCs, and in-vitro-activated T cells (Garrett-Sinha, 2013; Lattin et al., 2008; Wu et al., 2016). Ets1 function is important in immune homeostasis: Ets1 plays a role in the maintenance of Treg cell identity and suppresses PC and Th17 cell differentiation. Mechanistically, Ets1 maintains the Foxp3 locus in an open-chromatin conformation, and it also suppresses Blimp1 transcription and recruits NFAT to the II2 promoter to suppress PC and Th17 differentiation, respectively (John et al., 2008; Mouly et al., 2010; Tsao et al., 2013). Single-nucleotide polymorphisms (SNPs) in ETS1 are thought to contribute to SLE via these pathways; however, such assumptions are yet to be confirmed.

Tfh cells are a recent addition to the list of T cell subsets (Crotty, 2011). Tfh cell differentiation requires IL-6, IL-21, and ICOS signaling, which turns on the expression of Tfh-cell-polarizing factors (such as *Bcl6*, *Ascl2*, and *Batf*), whereas Tfh-cell-suppressive factors (such as *II7ra* and *Klf2*) are turned off. Mature Tfh cells migrate into germinal centers (GCs) via signaling by the chemokine receptor CXCR5. At the GC, Tfh cells interact with



<sup>&</sup>lt;sup>2</sup>Division of Integrative Biosciences and Biotechnology, Pohang University of Science and Technology, Pohang, Gyeongbuk 37673, Republic of Korea

<sup>&</sup>lt;sup>3</sup>Department of Rheumatology, Ajou University School of Medicine, 164 Worldcup-ro, Yeongtong-gu, Suwon, Gyeonggi-do 16499, Republic of Korea

<sup>&</sup>lt;sup>4</sup>Lead Contact

<sup>\*</sup>Correspondence: iimsh@postech.ac.kr https://doi.org/10.1016/j.immuni.2018.10.012

B cells through co-stimulatory molecules, such as ICOS, CD40L, and interleukin 4 (IL-4) and IL-21 signaling, to ultimately guide the processes of B cell affinity maturation and PC differentiation (Vinuesa et al., 2016). In line with their key role in activating B cells, Tfh cell numbers are increased in patients suffering from B-cell-related autoimmune diseases, such as SLE, rheumatoid arthritis, and Sjögren's syndrome, and exhibit features of a highly activated state (Vinuesa et al., 2016). Thus, Tfh cells are a promising target for immunotherapy in B-cell-related autoimmune disease, and understanding the mechanics that contribute to Tfh cell dysregulation will contribute to this endeavor.

Here, we examined the role of Ets1 in different cell types associated with SLE. We found that genetic deletion of *Ets1* in CD4<sup>+</sup> T cells, but not in B cells or dendritic cells (DCs), recapitulated SLE-like autoimmunity. Deletion of Ets1 in CD4<sup>+</sup> T cells resulted in the expansion of IL-4-secreting GATA-3<sup>+</sup>Bcl6<sup>+</sup> Tfh type 2 (Tfh2) cells, which induced the production of self-reactive IgE and IgG1. Mechanistically, Ets1 suppressed Tfh2 differentiation by regulating the expression of Tfh and Th2 skewing factors. Tfh2 frequencies in SLE patients correlated with disease parameters, providing evidence for the relevance of these findings to our understanding of human disease.

#### **RESULTS**

# Development of SLE-like Autoimmunity in Ets1 $^{\Delta CD4}$ Mice

We first confirmed that germline Ets1-/- mice developed SLElike autoimmunity in our animal facility maintained under specific-pathogen-free conditions as previously reported (Wang et al., 2005) (Figures S1A-S1E). To dissect which type of immune cells play key roles in disease development, we generated mice where exon 7 of Ets1, encoding a DNA binding domain of Ets1, was flanked by two loxp sites (Ets1 flox mice). Next, we generated cell-type-specific Ets1-deficient mice where Ets1 was deleted in T cells (Ets1 $^{\Delta CD4}$ ), B cells (Ets1 $^{\Delta CD19}$ ), and DCs (Ets1 $^{\Delta CD11c}$ ) (Figure S1F). SLE-like autoimmunity was observed only in Ets1<sup>ΔCD4</sup> mice. At week 7, Ets1<sup>\text{\DOD4}</sup> mice displayed splenomegaly, lymphadenopathy, activation of T cells, glomerulonephritis, and skin lesions, which are all key symptoms of SLE (Figures 1A-1E and S1G-S1I). With age, 70% of Ets1<sup>\text{\text{DCD4}}</sup> mice developed skin lesions, and their life expectancy dropped to 25% lower than that of littermate controls (Figures 1F and 1G). In contrast, Ets1<sup>\(\Delta\CD19\)</sup> and Ets1<sup>\(\Delta\CD11c\)</sup> mice exhibited no distinct abnormalities, indicating that autoimmunity is initiated by T cells under Ets1 deficiency.

 $Ets1^{\Delta CD4}$  mice also had a dysregulated B cell phenotype. Although no difference was observed in T cell numbers (Figure 1H), absolute B cell numbers were significantly increased (Figure 1I) with upregulation of activation markers (Figures 1J and S1J). Moreover, high levels of anti-dsDNA IgG autoantibodies (which are known to form immune complexes that deposit at kidney and skin, causing tissue damage [Figures 1L and 1M]) were detected in the serum of  $Ets1^{\Delta CD4}$  mice (Figure 1K) (Reichlin and Wolfson-Reichlin, 2003). These findings suggest that loss of Ets1 in T cells initiates autoimmunity by enhancing T-cell-dependent autoantibody-mediated tissue damage.

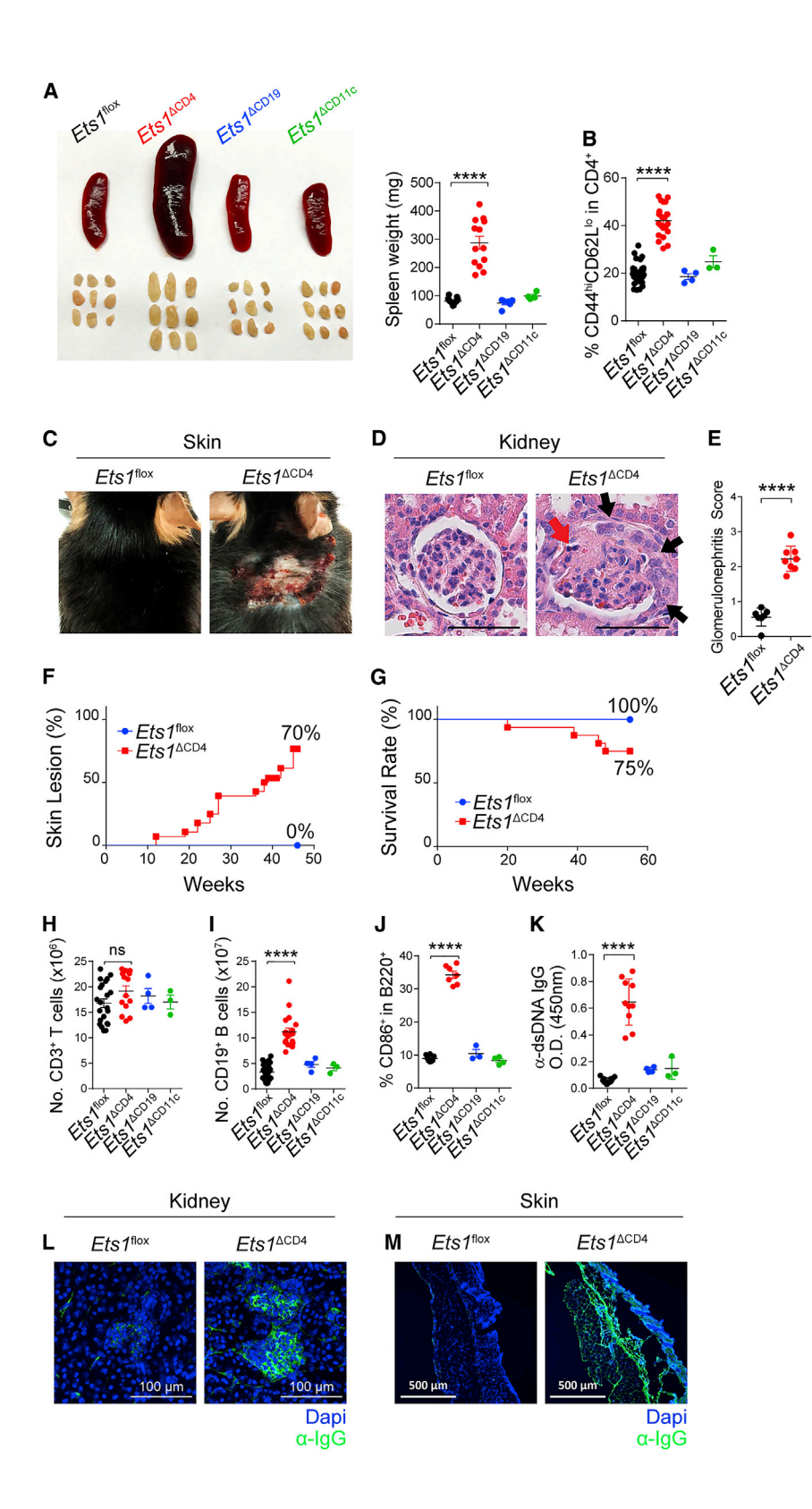
# Increased Numbers of Tfh Cells and GC Responses in Ets1 $^{\Delta \text{CD4}}$ Mice

Tfh cells are the major helpers for activation and differentiation of antigen-specific B cells, which are associated with B-cell-linked autoimmune diseases. Therefore, we hypothesized that a spontaneous increase in Tfh cell numbers might have caused humoral autoimmunity in Ets1 <sup>\text{\DCD4}</sup> mice. Indeed, CD4 +CXCR5 +PD-1 + Tfh cells were significantly more abundant in  $Ets1^{\Delta CD4}$  mice than in controls (Figure 2A). These cells expressed high numbers of key Tfh cell markers, such as the transcription factor Bcl6 (Johnston et al., 2009) and the cytokine IL-21 (Figures S2A-S2C). Moreover, the Tfh cells seemed functional given that the population of CD19+GL7+CD95+ GC B cells was significantly increased (Figure 2B) and spontaneous GCs were formed in the spleens of Ets1<sup>\text{\DeltaCD4}</sup> mice (Figure 2C). Linear regression analysis further confirmed a positive correlation between Tfh and GC B cell numbers (Figure 2D). Of note, Tfh cells positively correlated with GC B cells in wild-type (WT) mice as well (Figures S2D and S2E). In contrast, Th1, Th2, and Th17 cells did not show any correlation with GC B cell frequencies, although Th1 and Th2 cells were increased in Ets1<sup>\(\Delta\)</sup>CD4 mice (Figures S2F-S2N). Ets1 is known to suppress Th17 differentiation (Figures S2M and S2N); however, Th17 cells did not correlate with GC B cell numbers regardless of whether they were analyzed as RORγt+ or IL-17A+ cells, suggesting that they are not involved with humoral autoimmunity (Figures S2J and S2L), Finally, there was an increase in CD138+B220- PCs, which correlated with Tfh and GC B cell frequencies in Ets1<sup>\text{\DOD4}</sup> mice (Figures 2E-2G).

Even though Th cells other than Tfh cells did not show a correlation with disease severity, we utilized adoptive-transfer experiments to confirm this. In brief, CD19+CD138- B cells, CD4+GITR-CXCR5-CD44+CD62L- activated T (Tem) cells, and CD4<sup>+</sup>GITR<sup>-</sup>CXCR5<sup>+</sup>PD-1<sup>+</sup> Tfh cells were sorted from *Ets1*<sup>ΔCD4</sup> mice and transferred to lymphocyte-deficient Rag1-mutant mice ( $Rag1^{-/-}$ ) (Figure 2H). A total of three groups were made: B cell. B + Tem cell. and B + Tfh cell. We analyzed the mice 7 weeks after transfer and discovered GC B cell induction and an increase in serum IgG and serum α-dsDNA IgG exclusively in the B + Tfh cell transfer group (Figures 2I-2K). Moreover, there were immune complex depositions in the glomeruli and increased albuminuria, an indication of leaky glomeruli, in B + Tfh cell transfer groups but not the remaining two groups (Figures 2L and 2M). This suggests that Th1 and Th2 cells were increased but irrelevant to autoantibody-mediated SLE pathogenesis in  $Ets1^{\Delta CD4}$  mice.

# Subset-Specific Increase in Tfh2 Cells in Ets1 $^{\Delta CD4}$ Mice

When analyzing the concentration of serum immunoglobulin in  $Ets1^{\Delta CD4}$  mice, we noticed that hyperglobulinemia was skewed primarily toward a type 2 response; the concentrations of IgG1 and IgE were 79- and 12,000-fold higher than normal, respectively, whereas the concentrations of IgG2b and IgG3 were 1.6- and 2.9-fold higher than normal, respectively. (Table S1). This result prompted us to test whether Tfh cells were biased toward a Tfh2 phenotype. We tested this possibility by employing the strategy used to analyze human blood Tfh subsets; in brief, after being gated on Tfh cells, Tfh1 (CXCR3+CCR6-), Tfh2 (CXCR3-CCR6-), and Tfh17 (CXCR3-CCR6+) cells were analyzed accordingly (Figure 3A) (Morita et al., 2011). We found that Tfh2 cells were highly increased at the expense of Tfh1 and



Tfh17 cells in the spleens of  $Ets1^{\Delta CD4}$  mice (Figure 3B). Cytokine expression followed this pattern, such that IL-4 saw the biggest increase, whereas IFN $_{\Upsilon}$  and IL-17A saw mild increases in Tfh cells of  $Ets1^{\Delta CD4}$  mice (Figure S2O). Because the chemokine-re-

Figure 1. Development of SLE-like Autoimmunity in  $\it Ets1^{\Delta CD4}$  Mice

- (A) Representative images (left) of spleen and lymph nodes of  $Ets1^{flox}$  (black),  $Ets1^{\Delta CD1e}$  (red),  $Ets1^{\Delta CD1e}$  (blue), and  $Ets1^{\Delta CD11c}$  (green) mice, as well as a summary graph (right).
- (B) Frequencies of CD4<sup>+</sup>CD42<sup>hi</sup>CD62L<sup>lo</sup> T effector cells detected from spleens of indicated mice as determined by flow cytometry.
- (C) Representative images of skin lesions detected in facial, neck, and dorsal regions of  $Ets1^{\Delta CD4}$  mice at 28 weeks of age.
- (D) Representative light microscopy images of glomeruli of Ets1<sup>flox</sup> and Ets1<sup>ΔCD4</sup> mice at 28 weeks of age after hematoxylin and eosin staining. Crescent (black arrows) and sclerosis (red arrow) are indicated. Scale bars: 50 μm.
- (E) Summary graph of glomerulonephritis scoring of  $Ets1^{\Delta CD4}$  mice at 28 weeks of age.
- (F and G) Incidence of skin lesions (F) and survival rate (G) in  $Ets1^{flox}$  and  $Ets1^{\Delta CD4}$  mice over the indicated time period.
- (H–J) Absolute numbers of CD3<sup>+</sup> T cells (H) and CD19<sup>+</sup> B cells (I) and frequencies of CD86<sup>+</sup> B220<sup>+</sup> B cells (J) in the indicated mice as determined by flow cytometry.
- (K) Anti-double-stranded DNA ( $\alpha$ -dsDNA) IgG in serum of the indicated mice as determined by FLISA
- (L and M) Representative confocal microscopy images of IgG immune complex deposition (green) in the glomeruli (L) and skin (M) of  $Ets1^{\rm flox}$  and  $Ets1^{\rm ACD4}$  mice. DAPI staining is indicated in blue. Data from flow cytometry and ELISA are representative of at least three independent experiments. Horizontal bars denote mean  $\pm$  SEM. For (A), (B), and (G)–(J), two-tailed unpaired Student's t test was used for statistical analyses:  $^{\rm tp} < 0.05, ^{\rm tp} < 0.01, ^{\rm ttp} < 0.001, ^{\rm ttp} < 0.0001$ . See also Figure S1.

ceptor gating strategy is not conventional in mice, we validated whether these were bona-fide Tfh2 cells. Indeed, Tfh2 cells in Ets1<sup>\text{\text{DD4}}</sup> mice expressed the Tfh signature molecules ICOS, IL-21, and Bcl6 and the Th2 signature molecules IL-4, IL-13, and GATA-3 (Figures 3C-3E and S3A-S3C). Tfh2 cells from WT mice, however, expressed ICOS, IL21, and Bcl6 but not IL-4 or GATA-3, suggesting that they were not true Tfh2 cells (Figures 3C, 3D, and S3A-S3C). This put the chemokinegating strategy under question, so we tested a new gating strategy (GATA-3+Bcl6+). GATA-3+Bcl6+ Tfh2 cells were highly increased in Ets1 ACD4 mice but were minimally detected in WT mice,

proving its reliability for analyzing murine Tfh2 cells (Figure 3F). Next, we tested the functional capacity of individual Tfh subsets. We used correlation analysis as a measurement of functionality and found that GATA-3<sup>+</sup>Bcl6<sup>+</sup> Tfh2 cells and IL-4<sup>+</sup> Tfh2 cells

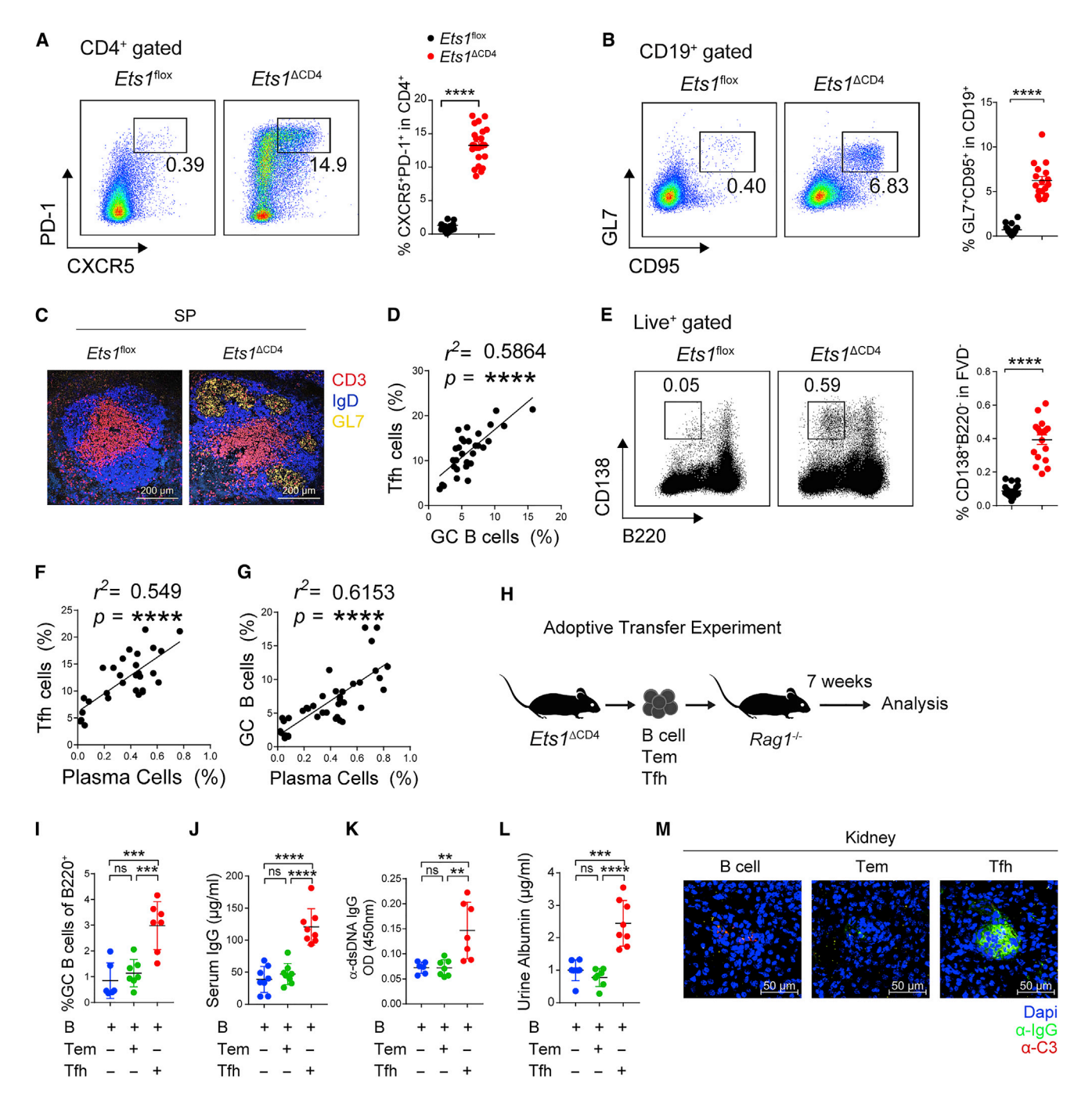


Figure 2. Enhanced Tfh Cell and Germinal Center Responses in  $\textit{Ets1}^{\Delta CD4}$  Mice

(A and B) Flow-cytometric plots (left) and summary graph (right) of T follicular helper (Tfh) cells (A) and germinal center B (GC B) cells (B) in the spleens of Ets1<sup>flox</sup> and  $Ets1^{\Delta CD4}$  mice at 6–8 weeks of age.

(C) Representative images of GL7+ GCs (yellow) within IgD+ B cell follicles (blue) in the spleens of Ets1<sup>flox</sup> and Ets1<sup>aCD4</sup> KO mice as analyzed by confocal microscopy. CD3+ T cell zones are marked in red.

(D) Correlation analysis of Tfh and GC B cell frequencies in individual immune organs (peripheral lymph nodes, mesenteric lymph nodes, and spleens) of  $Ets1^{\Delta CD4}$ 

(E) Flow-cytometric plots (left) and summary graph (right) of plasma cells (PCs) in the spleens of Ets1<sup>flox</sup> and Ets1<sup>ΔCD4</sup> mice at 6–8 weeks of age.

(F and G) Correlation analysis of Tfh cell and PC frequencies (F) and of GC B cell and PC frequencies (G) in individual immune organs (peripheral lymph nodes, mesenteric lymph nodes, and spleens) of  $Ets1^{\Delta CD4}$  mice (n = 7). (H–M) B, Tem, and Tfh cells were sorted from  $Ets1^{\Delta CD4}$  mice and transferred to  $Rag1^{-/-}$  hosts intravenously. Mice were analyzed 7 weeks later.

(H) Summary diagram of experimental scheme.

positively correlated with GC B cells (Figures 3G and 3H), but IFN $\gamma^+$  Tfh1 cells, IL-17A<sup>+</sup> Tfh17 cells, and CD4<sup>+</sup>GATA-3<sup>+</sup>Bcl6<sup>-</sup> Th2 cells did not (Figures S3D–S3F), although a few showed tendencies of correlation, suggesting that Tfh2 cells are most influential in shaping the GC response in *Ets1*<sup> $\Delta$ CD4</sup> mice.

Next, to verify that type 2 hyperglobulinemia in  $Ets1^{\Delta CD4}$  mice is Tfh2 dependent, we performed in vitro T cell-B cell co-culture assays by using Tfh (CD4+CXCR5+PD-1+), Tem (CD4+  $\text{CXCR5}^-\text{CD44}^+\text{CD62L}^-)\text{,}$  and total  $\text{CD4}^+$  (CD4 $^{\text{To}}\!)$  cells, each sorted from WT or Ets1 ACD4 mice, and co-cultured them individually with B220<sup>+</sup> B cells (Sage and Sharpe, 2015). After 6 days of culture, secreted IgE amounts were measured from the culture supernatants by ELISA. CD4To and Tfh cells isolated from Ets1<sup>\text{\DeltaCD4}</sup> mice induced IgE isotype switching; however, Tem cells from  $\mathit{Ets1}^{\Delta CD4}$  mice and all T cell groups isolated from WT mice failed to induce IgE isotype switching, but they could induce IgG responses (Figures 3I and S3G). It is worth noting that although Tem groups had high frequencies of IL-4-secreting cells (Figure S2K), they were unable to induce IgE isotype switching in B cells. One explanation could be that Tem cells are less capable than Tfh cells of activating B cells (Figures S3H-S3K).

To test whether Tfh2 cells were responsible for the autoimmune IgE response in vivo, we first checked which Tfh cell subset correlated with the expansion of IgE+ GC B cells (Figures 3J and 3K). GATA-3+Bcl6+ Tfh2 cells and IL-4+ Tfh2 cells both showed a positive correlation with IgE+ GC B cells (Figures 3L and 3M). In contrast, IFN- $\gamma^+$  Tfh1 or IL-17A<sup>+</sup> Tfh17 cells showed no correlation with the expansion of IgE+ GC B cells (Figures S3L and S3M). Next, to see whether IgE and IgG1 had autoimmune functions, we checked for self-reactive antibodies. Indeed, anti-dsDNA IgE and anti-dsDNA IgG1 autoantibodies were highly increased in the serum of  $Ets1^{\Delta CD4}$  mice (Figure 3N), and immune deposits, which overlapped complement 3 (C3) depositions, signifying ongoing inflammation, were readily visualized in the skin and kidney of Ets1 ACD4 mice (Figures 30-3R, S3N, and S3O). Thus, Tfh2 cells could induce IgE isotype switching in B cells and were responsible for the autoimmune type 2 hyperglobulinemia found in  $Ets1^{\Delta CD4}$  mice.

# Ets1 Deficiency in Treg Cells Does Not Cause Humoral Autoimmunity

Next, we sought to understand the cellular mechanisms behind the increase in Tfh cells in  $Ets1^{\Delta \text{CD4}}$  mice. Because Ets1 is involved in maintaining Treg cell stability and deficiencies of Treg cells or T follicular regulatory (Tfr) cells lead to humoral autoimmunity (Fu et al., 2018; Lin et al., 2005), we tested whether a defect in Treg cells causes SLE symptoms in  $Ets1^{\Delta \text{CD4}}$  mice. However, rather than being decreased, Tfr cells were increased in  $Ets1^{\Delta \text{CD4}}$  mice, and they did not show any correlative relation to Tfh cell frequencies (Figures S4A–S4C). Moreover, *in vitro* functional assays of WT and Ets1-deficient Tfr cells showed comparative suppressive capacity, signifying that Ets1-deficient

Tfr cells were functional (Figure S4D). Furthermore, we generated Treg-cell-specific Ets1-deficient mice ( $Ets1^{\Delta Foxp3}$ ) and discovered that  $Ets1^{\Delta Foxp3}$  mice did not have dysregulation of Tfh cells or GC B cells or increases in serum IgG or IgE autoantibodies in comparison with  $Ets1^{\Delta CD4}$  mice (Figures S4E–S4H). Thus, Ets1 deficiency in Treg cells was not sufficient to induce the humoral autoimmunity seen in  $Ets1^{\Delta CD4}$  mice.

# Enhanced Differentiation of Tfh2 Cells under Ets1 Deficiency

We next focused on cell-intrinsic mechanisms that could have caused the increase in Tfh cells. Three scenarios were envisioned: increased proliferation, decreased apoptosis, and enhanced differentiation of naive T (Tn) cells into Tfh cells. Tfh cells isolated from Ets1<sup>ACD4</sup> mice showed slightly increased proliferation (Figure S4I), whereas ex-vivo-isolated Tfh cells from WT and Ets1<sup>ACD4</sup> mice showed comparable apoptosis (Figures S4J and S4K).

To check whether deletion of Ets1 results in increased Tfh cell differentiation, we performed adoptive-transfer experiments (Figure S4L) (Park et al., 2017). In brief, naive ovalbumin (OVA)-specific CD4+ T cells were isolated from OT-II TCR tg Ets1<sup>flox</sup> (OT-II WT) or OT-II TCR tg Ets1<sup>ΔCD4</sup> (OT-II knockout [KO]) mice, injected into congenic mice, immunized with alum-emulsified OVA (OVA-alum), and analyzed at later time points. At day 7 after immunization, we discovered significantly more (51.8-fold) Tfh cells in transferred OT-II KO cells than in OT-II WT cells (Figures 4A and 4B). This number far exceeded the ratio of increase between total OT-II KO and OT-II WT transferred cells (4.6-fold), which reflects the enhanced proliferative capacity of the transferred OT-II KO cells (Figure 4B).

We further analyzed whether the Tfh cells were skewed toward a Tfh2 cell phenotype. Indeed, transferred OT-II KO cells had a higher proportion of GATA-3+CXCR5+ cells than did OT-II WT cells (Figure 4C). Moreover, transferred OT-II Tfh cells expressed more GATA-3 than did Tem cells of the recipient mice, suggesting an intrinsic propensity of OT-II KO T cells to overexpress GATA-3 (Figure 4D). In terms of the B cell response, there was larger induction of GC B cells and higher serum concentration of OVA-specific IgE and IgG in OT-II KO transferred groups than in OT-II WT transferred groups (Figures 4E–4G). These results support the observations made in  $Ets1^{\Delta CD4}$  mice and suggest that an enhanced Tfh cell differentiation program might be the key cause of the high number of Tfh cells in  $Ets1^{\Delta CD4}$  mice.

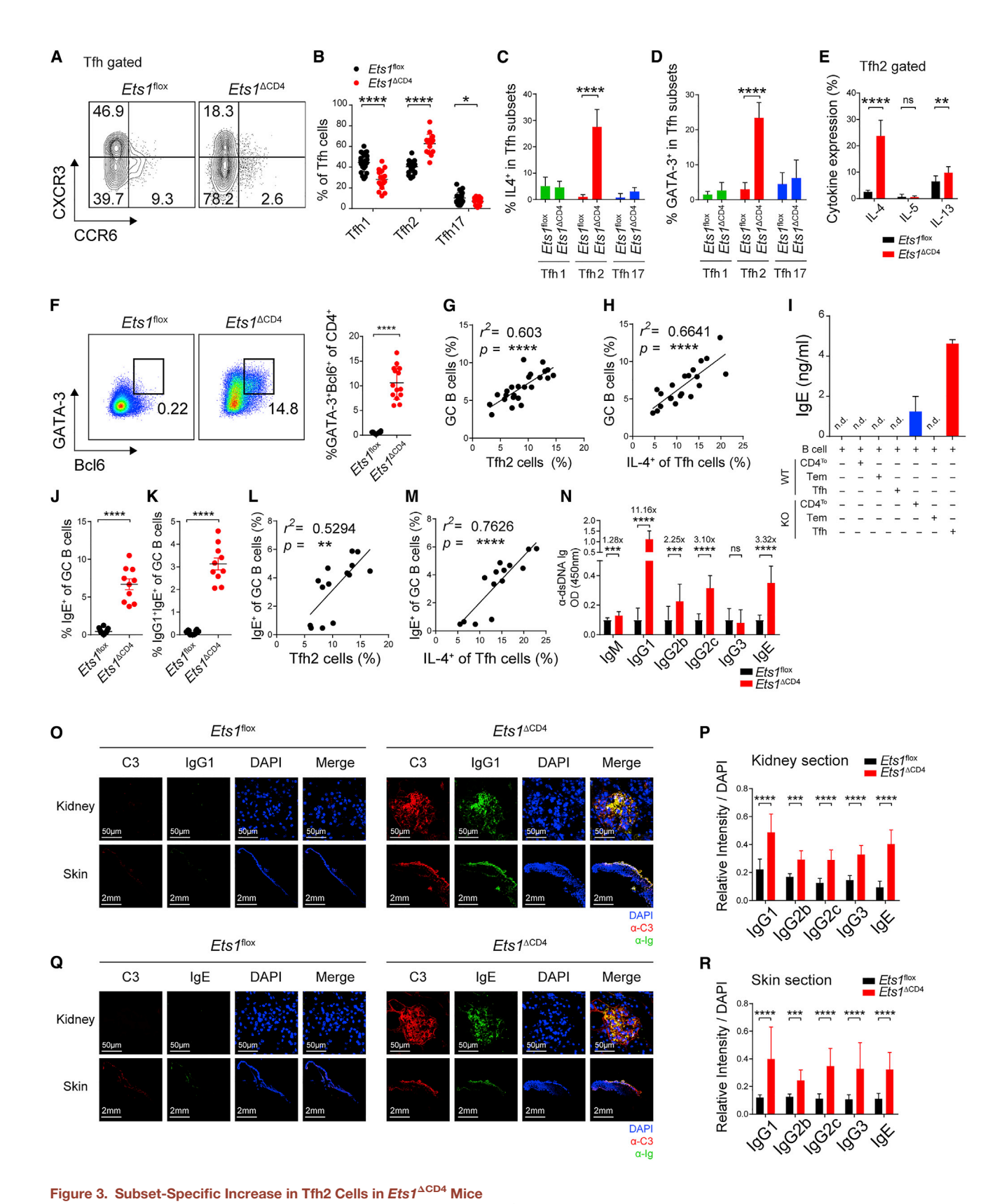
# Deregulation of Tfh Genes in Ets1<sup>ACD4</sup> T Cells

To elucidate the molecular mechanisms of Ets1-dependent Tfh cell regulation, we determined Ets1 expression between Tn, Tem, and Tfh cells. Ets1 was highly expressed in Tn and Tem cells but to a lesser degree in Tfh cells (Figure 5A). Thus, we hypothesized that Ets1 might suppress the expression of key Tfh cell genes in Tn cells, and its lack of binding to Tfh cell gene

<sup>(</sup>I–L) Summary graphs of GC B cell frequencies (I), serum IgG concentrations (J), serum α-dsDNA IgG concentrations (K), and urine albumin concentrations (L) in Rag 1 KO recipients.

<sup>(</sup>M) Representative confocal microscopy image of glomeruli in individual groups of Rag 1 KO recipients.

Data from glow cytometry and ELISA are representative of at least three independent experiments. Horizontal bars denote mean  $\pm$  SEM. For (A), (B), (E), and (I)–(L), a two-tailed unpaired Student's t test was used for statistical analysis: \*p < 0.05, \*\*p < 0.01, \*\*\*p < 0.001, \*\*\*\*p < 0.0001. Goodness-of-fit r² values for (D), (F), and (G) are indicated: \*p < 0.05, \*\*p < 0.01, \*\*\*p < 0.001, \*\*\*p < 0.001. See also Figure S2.



(A and B) Flow-cytometric plot of Tfh-cell-subset analysis in Ets1<sup>flox</sup> and Ets1<sup>ΔCD4</sup> mice (A) and summary graph (B). Cells were pre-gated on Tfh (CD4<sup>+</sup>PD1<sup>+</sup> CXCR5<sup>+</sup>) cells. Tfh1, CXCR3<sup>+</sup>CCR6<sup>-</sup>; Tfh2, CXCR3<sup>-</sup>CCR6<sup>-</sup>; and Tfh17, CXCR3<sup>-</sup>CCR6<sup>+</sup>.

loci could preferentially turn on the program of Tfh cell differentiation. To test this hypothesis, we performed mRNA transcriptome analysis in non-Tfh and Tfh cells isolated from WT mice (WT non-Tfh and WT Tfh, respectively) and Ets1<sup>\text{\DeltaCD4}</sup> mice (KO non-Tfh and KO Tfh, respectively). As expected, WT non-Tfh and Tfh cells separated into two distinct transcriptome profiles. KO non-Tfh cells, on the other hand, displayed an intermediate transcriptome profile leaning toward Tfh cells (Figures 5B and S5A). Of note, gene expression of key positive regulators of Tfh cell differentiation was increased in KO non Tfh cells, inducing Etv5 (Park et al., 2017), Egr2, Bcl6, P2rx7, and Batf (Figures 5B-5C and S5A) (Vinuesa et al., 2016). Gene-set enrichment analysis (GSEA) confirmed the enrichment of Tfh cell genes in the transcriptome of KO non-Tfh cells (Figure 5D). We also compared gene expression profiles of WT Tfh and KO Tfh cells and found that KO Tfh cells showed higher expression of Th2 cell genes, including II4 (Seder et al., 1992), Gata3, and IL13ra1 (Figures 5B, 5E, and S5B) (Zhu et al., 2010). In addition, the expression of factors involved in positive regulation of Tfh cell differentiation (Etv5, Bcl6, Icos, and Ascl2) was further increased, whereas that of negative regulators (KIf2, II7r, and Foxo1) was decreased in KO Tfh cells compared with WT Tfh cells (Figures 5B, 5E, and S5B) (Vinuesa et al., 2016). To determine whether deregulation of Tfh and Th2 cell signature genes occurs before or after activation of Tn cells, we analyzed mRNA expression of key Tfh and Th2 cell genes in Ets1-deficient Tn cells and saw upregulation of these genes even before they received activation signals (Figures 5F and 5G).

Next, we wished to determine whether Ets1 directly or indirectly regulates its target genes, and for this purpose we analyzed Ets1 chromatin immunoprecipitation sequencing (ChIP-seq) data in CD4+ T cells (Samstein et al., 2012). Ets1 was mainly enriched in the transcription start site (TSS) of Tfh cell genes, suggesting that Ets1 directly controls its target genes by binding to their promoters (Figure 5H). To understand whether Ets1 modulates the chromatin landscape of key Tfh cell genes, we subjected Tn and Tfh cells isolated from WT (WT Tn and WT Tfh, respectively) or Ets1<sup>ACD4</sup> (KO Tn and KO Tfh, respectively) mice to assay for transposase-accessible chromatin sequencing (ATAC-seq) (Buenrostro et al., 2015). Indeed, the chromatin status surrounding Tfh cell genes, including *Cxcr5*, *Bcl6*, *Ascl2*, *P2rx7*, *Tnfrsf4*, and *Ox40*, was in a more open structure in KO Tn cells than in WT Tn cells at a level comparable to

that of WT Tfh cells (Figures 5I–5J and S5C–S5F). To see whether the open chromatin structure correlated with enhanced protein expression, we measured amounts of Bcl6, ICOS, and CXCR5 in individual experimental settings. Indeed, amounts of Bcl6, ICOS, and CXCR5 were much higher in  $Ets1^{\Delta CD4}$  mice than in WT mice (Figures 5K–5L and S5G). Thus, Ets1 might directly bind to the regulatory regions of signature Tfh cell genes in Tn cells to suppress their pre-mature expression to block Tfh cell differentiation.

## Enhanced IL-4 Signaling in Ets1<sup>△CD4</sup> Mice

We next sought to understand the mechanisms underlying the Tfh2 cell bias seen in  $Ets1^{\Delta CD4}$  mice. IL-4 is a key cytokine involved in Th2 cell differentiation and T cell plasticity (Messi et al., 2003), therefore making it a good candidate for the underlying cause of enhanced IL-4+GATA-3+ Tfh2 cells in Ets1<sup>ACD4</sup> mice. As mentioned earlier, IL-4<sup>+</sup> Th2 cells were increased in  $Ets1^{\Delta CD4}$  mice, so there was an abundance of cytokine IL-4 (Figure 6A). In addition, Tfh cells expressed high amounts of IL-4, drawing a model of autocrine and paracrine IL-4 signaling (Figure 6B). In support, IL-4 receptor alpha (IL-4Rα) expression, phospho-STAT6 (pSTAT6) expression, and GATA-3 expressions were increased in Tn and Tfh cells of  $\mathit{Ets1}^{\Delta CD4}$  mice, suggesting ongoing IL-4 signaling (Figures 6C-6H). B cells in Ets1<sup>\text{\Delta}CD4</sup> mice also had elevated IL-4Rα and pSTAT6 expression, suggesting that IL-4 might act on both T cells and B cells (Figures 6I and 6J). Ets1 ChIP-seq results from CD4+ T cells showed that Ets1 might directly regulate II4ra expression by binding to the II4ra locus (Figure 6K). Moreover, ATAC-seg analysis revealed higher chromatin accessibility at the II4ra locus in KO Tn and KO Tfh cells (Figure 6K). Together, these results suggest that in the absence of Ets1, de-repressed Il4ra expression leads to enhanced IL-4 signaling and causes preferential Th2 and Tfh2 cell formation.

# IL-4 Neutralization Alleviates Disease Parameters in $Ets1^{\Delta CD4}$ Mice

On the basis of these results, we hypothesized that the increased production of IL-4 might be the underlying mechanism for disease pathogenicity in  $Ets1^{\Delta CD4}$  mice. Thus, we used IL-4-neutralizing antibodies to prove this notion. In brief, 5-week-old  $Ets1^{\Delta CD4}$  mice were treated with 1 mg of anti-IL-4 ( $\alpha$ -IL-4) or

<sup>(</sup>C) Summary graph of IL-4 expression in Tfh1 (green), Tfh2 (red), and Tfh17 (blue) gated cells in Ets1<sup>flox</sup> and Ets1<sup>ΔCD4</sup> mice.

<sup>(</sup>D) Summary graph of GATA-3 expression in Tfh1 (green), Tfh2 (red), and Tfh17 (blue) gated cells in Ets1<sup>flox</sup> and Ets1<sup>ΔCD4</sup> mice.

<sup>(</sup>E) Summary graph of IL-4, IL-5, and IL-13 expression in Tfh2 gated cells in Ets1<sup>flox</sup> and Ets1<sup>ΔCD4</sup> mice.

<sup>(</sup>F) Flow-cytometric plot of GATA-3<sup>+</sup>Bcl6<sup>+</sup> Tfh2 cells in Ets1<sup>flox</sup> and Ets1<sup>ΔCD4</sup> mice (left) and summary graph (right).

<sup>(</sup>G and H) Correlation analysis of GC B cells and GATA-3+Bcl6+Tfh2 cells (G) and of GC B cell-IL-4+Tfh cell (H) in the spleens of Ets1<sup>flox</sup> and Ets1<sup>ΔCD4</sup> mice.

<sup>(</sup>I) IgE concentration in the supernatants of B cell-T cell co-culture experiments as detected by ELISA. n.d., not detected.

<sup>(</sup>J and K) Summary graphs of IgE+ GC B cells (J) and IgG1+IgE+ GC B cells (K) in the spleens of Ets1+IoX and Ets1+OCD4 mice.

<sup>(</sup>L and M) Correlation analysis of IgE+GC B cell-GATA-3+Bcl6+Tfh2 cell frequencies (L) and of IgE+GC B cell-IL-4+Tfh cell frequencies (M) in the spleens of Ets1<sup>flox</sup> and Ets1<sup>ACD4</sup> mice.

<sup>(</sup>N) Summary graph of serum  $\alpha$ -dsDNA IgM, IgG1, IgG2b, IgG2c, IgG3, and IgE in  $Ets1^{flox}$  and  $Ets1^{\Delta CD4}$  mice as determined by ELISA.

<sup>(</sup>O and Q) Representative confocal microscopy images of skin and kidney sections of Ets1<sup>flox</sup> and Ets1<sup>ΔCD4</sup> mice. Staining: complement 3, red; DAPI, blue; IgG1, green (O); IgE, green (Q).

<sup>(</sup>P and R) Summary graphs of the intensity of IgG1, IgG2b, IgG2c, IgG3, and IgE deposits in the kidney (P) and skin (R) in relation to DAPI intensity.

Data from flow cytometry and ELISA are representative of at least three independent experiments. Horizontal bars denote mean  $\pm$  SEM. Data are represented as mean  $\pm$  SEM for (C)–(E), (I), (N), (Q), and (R). For (B)–(F), (J), (K), (N), (Q), and (R), a two-tailed unpaired Student's t test was used for statistical analysis: \*p < 0.05, \*\*p < 0.01, \*\*\*p < 0.001, \*\*\*p < 0.001, \*\*\*p < 0.001, \*\*\*p < 0.0001. See also Figure S3.

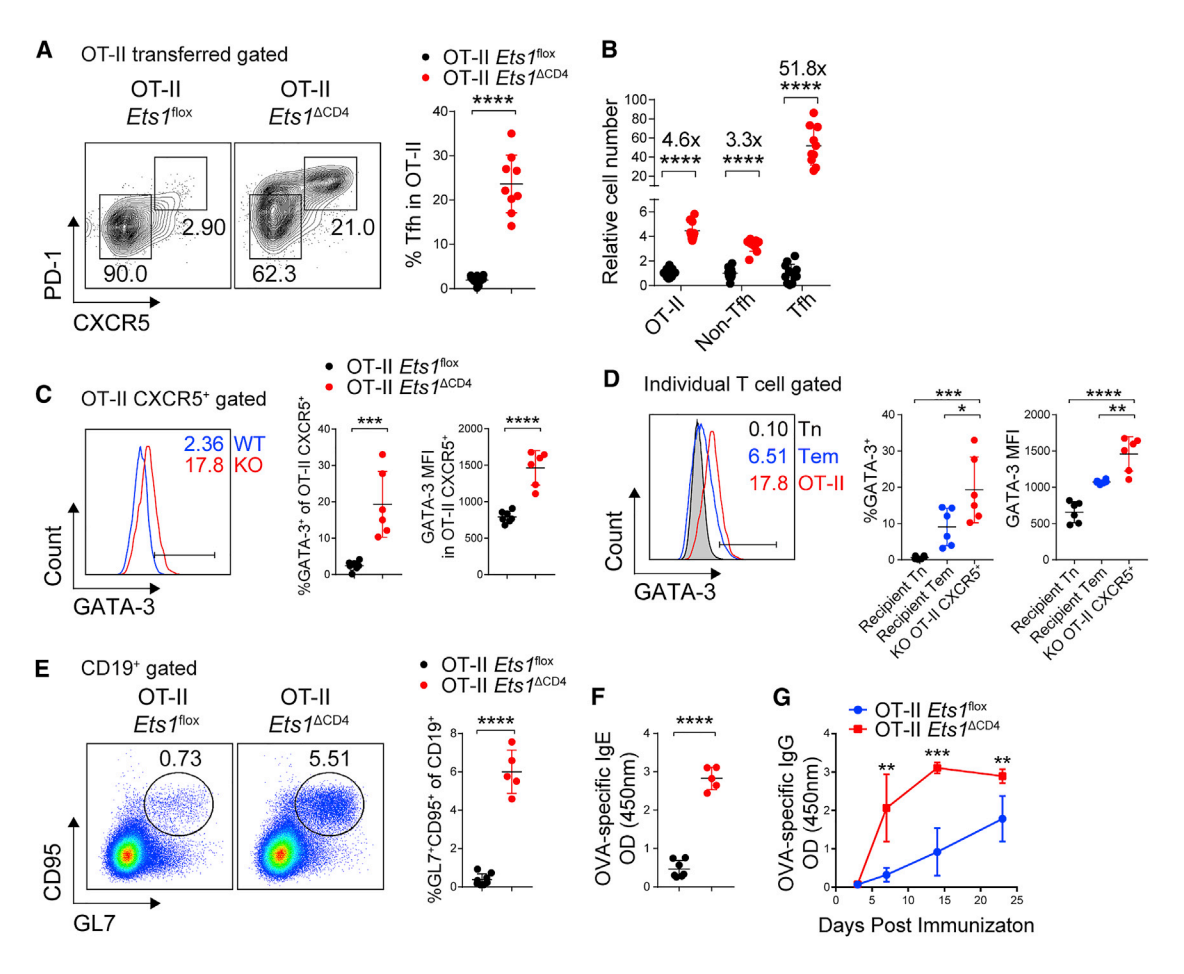


Figure 4. Enhanced Tfh2 Cell Differentiation of Ets1-Deficient Tn Cells

(A) Flow-cytometric plots (left) of Tfh and non-Tfh cells in transferred OT-II Ets1<sup>flox</sup> or OT-II Ets1<sup>ΔCD4</sup> cells and a summary graph (right).

(B) Relative numbers (OT-II KO and OT-II WT) of total transferred CD45.2<sup>+</sup> OT-II cells and relative numbers of non-Tfh gated and Tfh gated cells within CD45.2<sup>+</sup> OT-II cells are shown.

(C) Histogram of GATA-3 expression within CD4\*CD45.2\* (OT-II) CXCR5\* gated cells and summary graphs of GATA-3\* frequencies (middle) and GATA-3 MFIs (right) of the indicated groups.

(D) Histogram of GATA-3 expression within CD4+CD45.2-CXCR5-CD44-CD62L+ recipient T naive (Tn), CD4+CD45.2-CXCR5-CD44+CD62L- recipient Tem, and CD4+CD45.2+CXCR5+ KO OT-II cells within same host and summary graphs of GATA-3+ frequencies (middle) and GATA-3 MFIs (right).

(E) Flow-cytometric plots (left) of GC B cells in the indicated groups and a summary graph (right).

(F and G) OVA-specific IgE (F) and IgG (G) in the serum of the indicated groups as analyzed by ELISA.

For (A)–(G), a two-tailed unpaired Student's t test was used for statistical analysis: \*p < 0.05, \*\*p < 0.01, \*\*\*p < 0.001, \*\*\*\*p < 0.0001. See also Figure S4.

isotype control antibodies via the intraperitoneal route every day for 14 days (Figure 6L). IL-4 neutralization led to a significant smaller spleen size and lower absolute number of splenocytes in  $\alpha\text{-IL-4-treated}$  mice than in mice treated with isotype controls (Figures 6M and 6N). Also, whereas CD4+ Tem and Bcl6+ CXCR5+ Tfh cells were not reduced (Figures 6O and 6P), GATA-3+Bcl6+ Tfh2 cells were significantly decreased (Figure 6Q), proving that Tfh2 cell induction is IL-4 dependent. In terms of B cells, although the total frequencies of B cells were not altered (Figure 6R), the frequency of GC B cells, IgE+ GC B cells, and PCs were significantly reduced (Figures 6S-6U), and there was a complementary decline in serum concentrations of  $\alpha\text{-dsDNA}$  IgE (Figure 6V). Thus, IL-4 is involved in the induction of Tfh2 cells, GC B cells, and PCs, and neutralizing IL-4 cytokines show promising therapeutic value.

# **Downregulation of ETS1 Expression Correlates with Increased Human Tfh Cell Induction**

Mouse Ets1 and Human ETS1 share 97% amino acid identity (Garrett-Sinha, 2013), suggesting functional conservation. Thus, we tested the possibility that ETS1 suppresses Tfh cell differentiation in humans as well. For this purpose, Tn cells isolated from peripheral-blood mononuclear cells (PBMCs) of healthy donors were cultured under Tfh or Th0 cell differentiation conditions (Figure 7A) (Schmitt et al., 2014). We found that ETS1 amounts, measured by mean fluorescence intensity (MFI), were significantly lower in Tfh cells conditions than in Th0 cell conditions (Figure 7B). Moreover, under titrated Tfh cell differentiation conditions (TGF- $\beta$  titration) (Figure 7C), ETS1 expression showed inverse correlation with Tfh cell induction (Figure 7D). Molecularly, ETS1 ChIP-seq in human CD4+ T cells (Schmidl

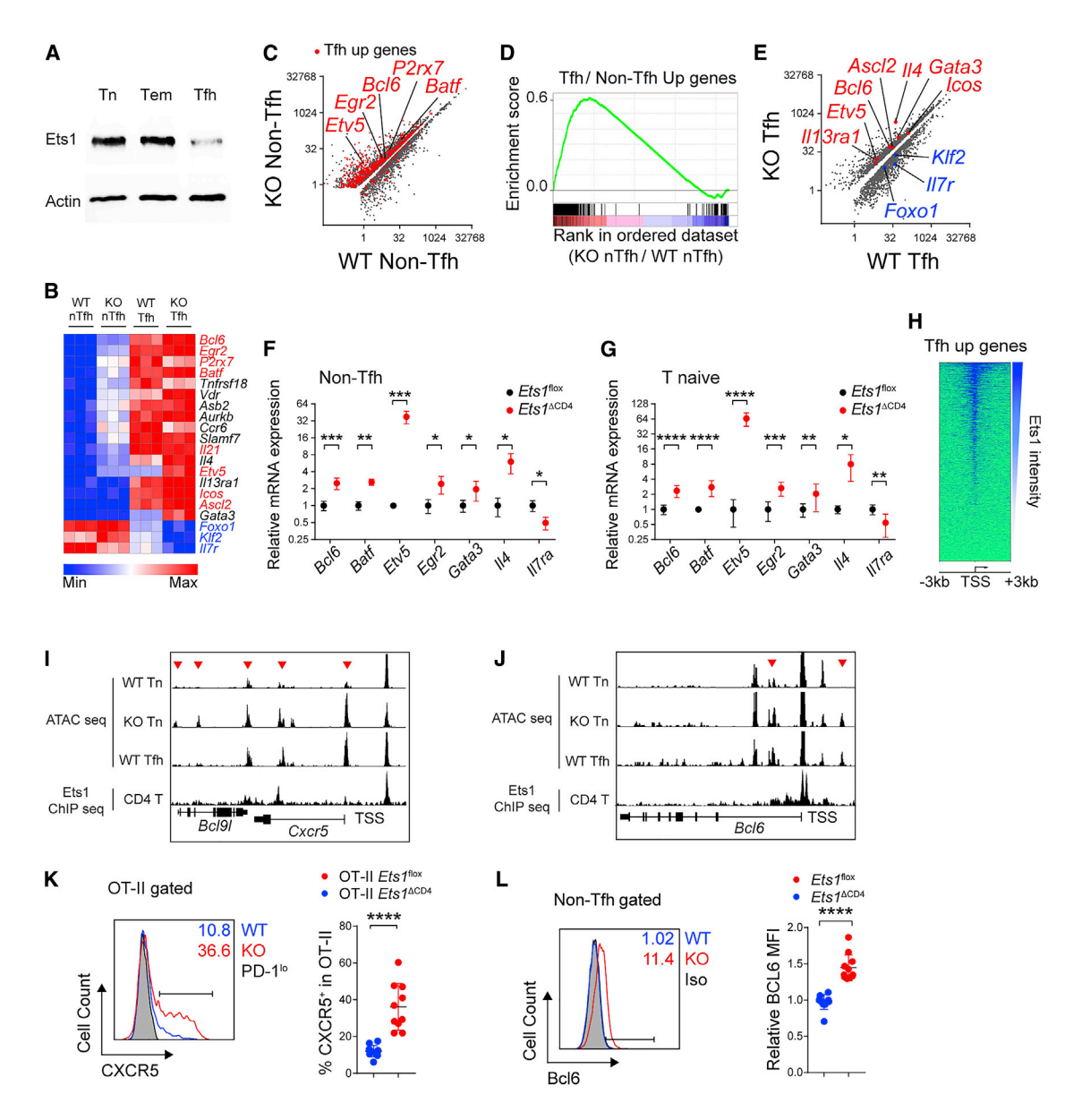


Figure 5. Deregulation of Tfh Cell Genes in Ets1-Deficient T Cells

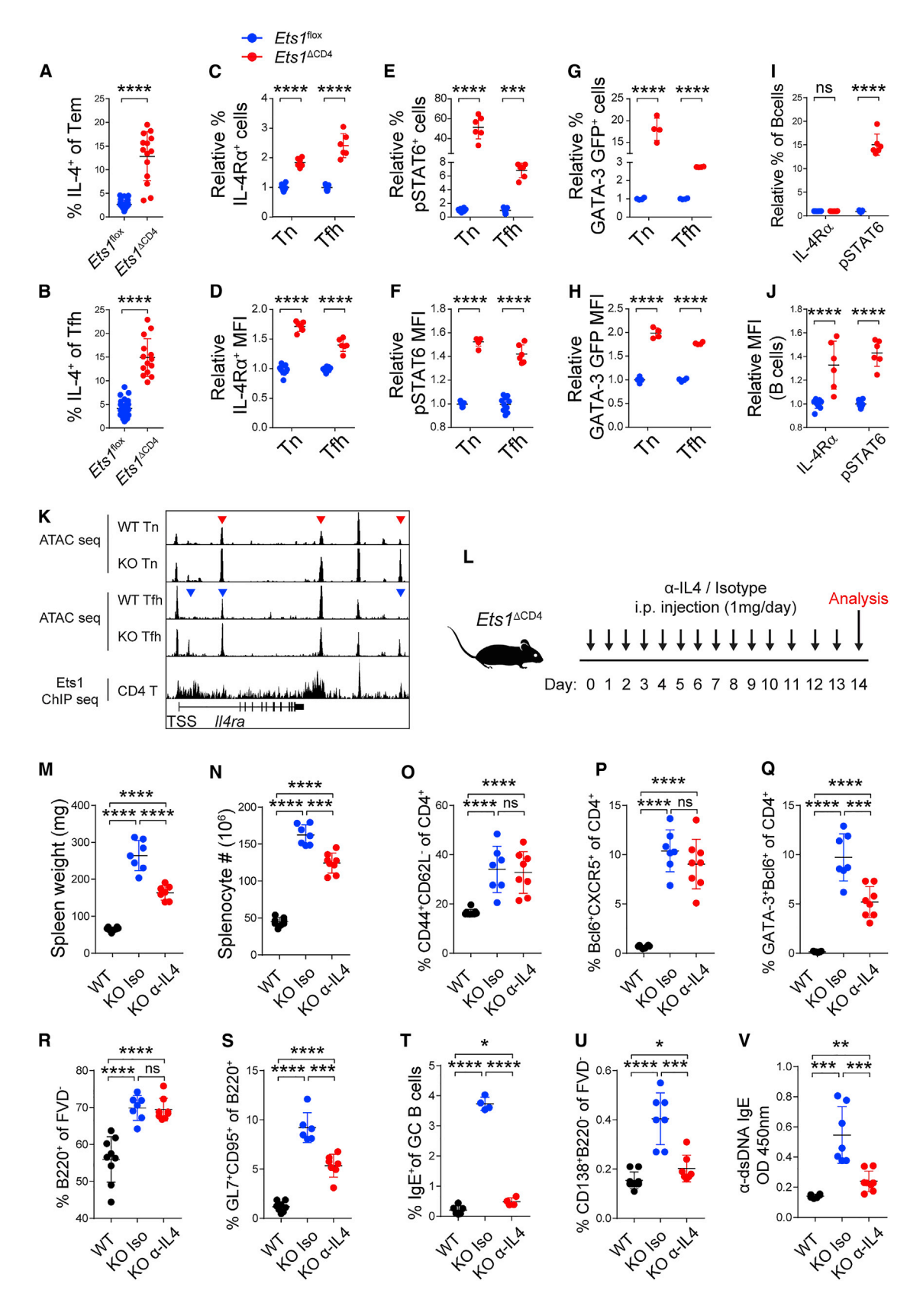
(A) Ets1 levels in Tn, Tem, and Tfh cells as detected by western blot.

(B) Heatmap of Tfh<sup>up</sup> and Tfh<sup>down</sup> cell genes in non-Tfh (nTfh) and Tfh cells isolated from Ets1<sup>flox</sup> (WT) and Ets1<sup>ΔCD4</sup> (KO) mice. Red, positive regulators of Tfh cell differentiation; blue, negative regulators of Tfh cell differentiation.

(C and E) Transcriptome profile of non-Tfh (C) and Tfh (E) cells sorted from  $Ets1^{\text{flox}}$  and  $Ets1^{\text{ACD4}}$  mice as analyzed by RNA sequencing (RNA-seq). Scatterplots of WT versus KO non-Tfh (C) and WT versus KO Tfh (E) gene expression profiles are shown. In (C) red dots represent differentially expressed genes (DEGs) when comparing WT Tfh divided by WT non-Tfh cells (log fold change > 1.5, in-house generated). In (E), red dots represent positive regulators of Tfh and Th2 cell differentiation, and blue dots represent negative regulators of Tfh cell differentiation.

- (D) GSEA of Tfh cell upregulated genes (in-house generated) within upregulated genes of KO non-Tfh versus WT non-Tfh cell transcriptomes.
- (F and G) Summary graphs of mRNA expression in non-Tfh cells (F) and Tn cells (G) isolated from  $Ets1^{flox}$  and  $Ets1^{\Delta CD4}$  mice.
- (H) Heatmap of Ets1 binding at the TSS  $\pm$  3 kb of Tfh cells genes as analyzed by ChIP-seq.
- (I and J) ATAC-seq signals in WT Tn, KO Tn, and WT Tfh cells along with Ets1 ChIP-seq signals at Cxcr5 (I) and Bcl6 (J) loci. ATAC-seq signals are normalized to Gapdh signals. Red arrows denote regions that display open structures in WT Tfh and KO Tn cells, but not in WT Tn cells.
- (K) Histogram of CXCR5 expression in transferred OT-II WT or OT-II KO Tn cells. WT PD-1<sup>low</sup> cells were used as negative controls (left). A summary graph of CXCR5<sup>+</sup> frequencies is also shown (right).
- (L) Histogram (left) of Bcl6 expression in non-Tfh cells of Ets1<sup>flox</sup> and Ets1<sup>ΔCD4</sup> mice. The isotype control is shown in grey (right). A summary graph of Bcl6 MFI is also shown (right).

Data from flow cytometry, western blots, and transfer experiments are representative of at least three independent experiments. Horizontal bars denote mean  $\pm$  SEM. Data are represented as mean  $\pm$  SEM for (F) and (G). For (F)–(H) and (J), a two-tailed unpaired Student's t test was used for statistical analysis: \*p < 0.05, \*\*p < 0.01, \*\*\*p < 0.001, \*\*\*\*p < 0.0001. See also Figure S5.



(legend on next page)

et al., 2014) showed that ETS1 binds to key Tfh cell gene loci, such as *BCL6*, *CXCR5*, *ICOS*, and *IL6R*, in patterns similar to those of murine Ets1 (Figures S6A–S6D). Thus, similar to its mouse counterpart (Ets1), human ETS1 seems to suppress Tfh cell differentiation in human CD4<sup>+</sup> T cells via suppressing the pre-mature expression of key Tfh cell genes.

# ETS1 Suppresses Tfh and Tfh2 Cells in Human SLE Patients

We further interrogated the involvement of ETS1 in human SLE pathogenesis. For this purpose, Korean SLE subjects (inactive SLE, SLE Disease Activity Index [SLEDAI] < 6, n = 58; active SLE, SLEDAI > 8, n = 19) and gender-matched healthy individuals (n = 62) were recruited (Table S2). Compared with healthy individuals, SLE patients showed lower ETS1 expression in CD4<sup>+</sup> T cells, and active SLE patients showed the lowest (Figure 7E). Furthermore, ETS1<sup>low</sup> (ETS1 MFI < 1,700) patients showed higher SLEDAI scores, higher serum anti-dsDNA titers, and lower serum C3 concentrations—the latter two of which are key immunologic parameters indicating active SLE (Lisnev-skaia et al., 2014)—than ETS1<sup>high</sup> (ETS1 MFI > 2,200) patients (Figure 7F and Table S3). Correlation analysis confirmed that these associations were significant and highly related (Figures 7G, S7A, and S7B).

We next compared the expression of ETS1 within individual Tfh cell subsets because this could signify a functional association. Blood Tfh cells consist of memory-like circulatory Tfh (cTfh) cells (CD4+CXCR5+CD45RA-), which can be dissected into Tfh1 (CXCR3+CCR6-), Tfh2 (CXCR3-CCR6-), and Tfh17 (CXCR3+CCR6-) cells. Upon analysis, we discovered that ETS1 expression was significantly lower in Tfh2 cells than in Tfh1 and Tfh17 cells regardless of whether we analyzed patient or healthy donor samples (Figures 7H, S7C, and S7D). This hinted at a specific role for ETS1, similar to its murine counterpart, in Tfh2 cell suppression. Indeed, ETS1 or patients showed higher frequencies of Tfh2 cells (Figure 7I and Table S3), whereas ETS1 MFI showed an inverse correlation with frequencies of Tfh2 cells (Figure 7J). In contrast, Tfh1 and Tfh17 cells showed no changes or correlation with ETS1 MFI (Figures S7E and S7F, and Table S3).

Previous studies have shown that an increase in Tfh2 cells is associated with disease severity in autoimmune patients (Ma et al., 2012). We asked whether Tfh2 cells are similarly related to disease severity of SLE (SLEDAI score). Indeed, Tfh2 cells were significantly increased in active SLE patients and positively correlated with disease severity (Figures 7K–7L and Table S4). In

contrast, Tfh1 and Tfh17 cells showed no associations with disease severity (Figures S7G-S7J). We also analyzed Treg and Tfr cells and found that Treg cell numbers were comparable but that Tfr cells were more abundant in SLE patients than in healthy control subjects (Figures S7K and S7L). Of note, blood Tfr cells are known to be indicators of ongoing humoral immunity (Fonseca et al., 2017); in support, Tfr cells positively correlated with serum α-dsDNA (Figure S7M). In terms of functionality, Tfh2 cells from SLE patients showed higher IL-4, IL-5, IL-13, and IL-21 expression than cells from control subjects, and IL-4 expression also correlated with SLEDAI scores (Figures 7M and 7N). To further prove heightened functionality, we sorted out Tfh2 cells from patient and healthy donors and did co-culture experiments with naive B cells (CD19<sup>+</sup>CD27<sup>-</sup>IgD<sup>+</sup>). We found that patient-derived Tfh2 cells induced more differentiation of naive B cells to plasmablasts and higher production of IgG from B cells, than did control-derived cells (Figures 70 and 7P). Finally, to test whether Tfh2 cells exacerbate autoimmune GC responses in SLE patients, we compared Tfh2 cell frequencies with serum  $\alpha$ -dsDNA titers. Indeed, an increase in Tfh2 cells positively correlated with serum α-dsDNA titers (Figure 7Q), whereas Tfh1 and Tfh17 cells showed no correlation (Figures S7N and S7O).

## **DISCUSSION**

SLE is a genetically driven autoimmune disease characterized by B-cell-derived autoantibodies. In this study, we assessed how mutation in the SLE susceptibility gene, *Ets1*, initiates autoimmunity and discovered that Ets1 can directly suppress signature Tfh and Th2 cell genes and thereby inhibit Tfh2 cell differentiation implicated in SLE-associated pathogenesis in mice and humans.

The transcription factor Ets1 is implicated in various immune pathways, including suppression of PC and Th17 cell differentiation and maintenance of Treg cell identity. This study adds Tfh and Tfh2 cells to the list of cells regulated by Ets1. Through our cell-type-specific *Ets1*-deletion experiments, we identified that Tfh and Tfh2 cells, but not Th1, Th2, or Th17 cells, are responsible for driving humoral autoimmunity in *Ets1*-/- mice. This is in contradiction to the previous notion, which inferred that dysregulation of Th17 cells, PCs, and Treg cells contributes to SLE autoimmunity in Ets1-deficient conditions. We, however, would like to point out that our report does not negate these possibilities. Th17 cells are more linked to lupus nephritis than to systemic autoimmunity (Martin et al., 2014), and the majority of our work was done in secondary lymphoid organs; therefore,

# Figure 6. IL-4 Neutralization Alleviates Disease in $Ets1^{\Delta CD4}$ Mice

(A and B) Summary graphs of IL-4 expression within CD4+CXCR5-CD44+ activated T cells (A) and Tfh cells (B) in Ets1<sup>flox</sup> and Ets1<sup>ACD4</sup> mice.

(C–H) Summary graphs of frequencies and MFIs of IL-4R $\alpha$  (C and D) pSTAT6-Y641 (E and F) and GATA-3-GFP (G and H) in the indicated cells of  $Ets1^{flox}$  and  $Ets1^{\Delta CD4}$  mice.

(I and J) Summary graphs of IL-4Ra and pSTAT6-Y641 expression in frequencies (I) and MFI values (J).

(K) ATAC-seq signals in WT Tn, KO Tn, WT Tfh, and KO Tfh cells along with Ets1 ChIP-seq signals at the *II4ra* locus. ATAC-seq signals were normalized by group for WT versus KO Tn cells and WT versus KO Tfh cells. Red arrows and blue arrows denote regions displaying open structures in KO Tn and KO Tfh cells, respectively, compared with WT counterparts.

(L–V)  $Ets1^{\Delta CD4}$  mice were injected intraperitoneally with 1 mg of  $\alpha$ -IL-4 or 1 mg of isotype control every day for 14 days.

(L) Summary figure of experimental scheme.

(M–V) Summary graphs of spleen weight (M), splenocyte numbers (N), CD4 $^+$  Tem cell frequencies (O), Tfh cell frequencies (P), Tfh2 cell frequencies (Q), B cell frequencies (R), GC B cell frequencies (S), IgE $^+$  GC B cell frequencies (T), PC frequencies (U), and  $\alpha$ -dsDNA IgE titers (V) in the indicated groups.

Data from flow cytometry and ELISA at a are representative of at least three independent experiments. Horizontal bars denote mean  $\pm$  SEM. For (A)–(F) and (I)–(R), a two-tailed unpaired Student's t test was used for statistical analysis: \*p < 0.05, \*\*p < 0.01, \*\*\*p < 0.001, \*\*\*\*p < 0.0001.

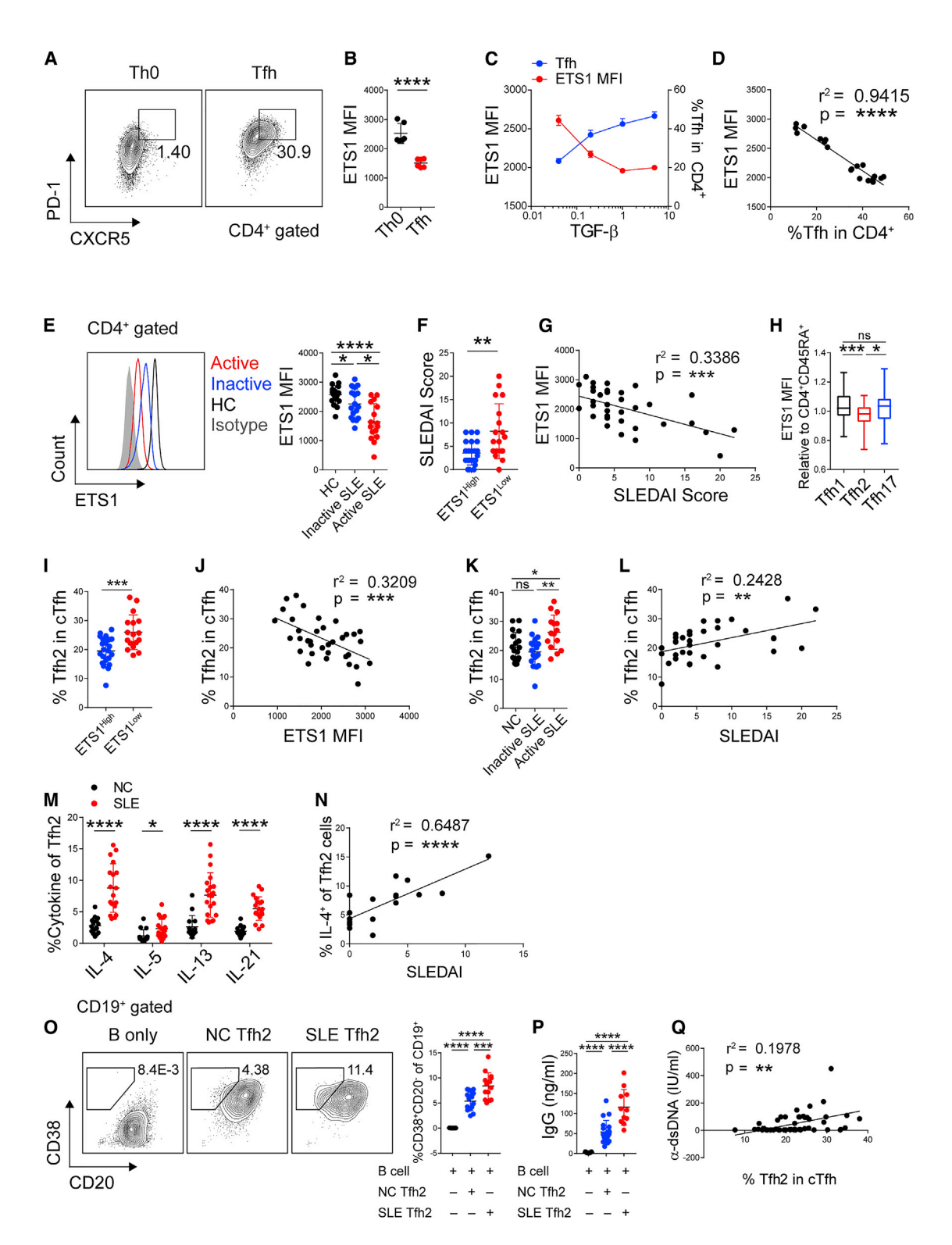


Figure 7. ETS1 Suppresses Tfh and Tfh2 Cells in Human SLE Patients

(A-D) Tn cells were isolated from the PBMCs of healthy donors and cultured under Th0 or Tfh cell differentiation conditions (A and B) or under TGF- $\beta$ -titrated Tfh cell differentiation conditions (C and D).

(A and B) Flow-cytometric plot of Tfh and Th0 cells (A) and summary graph of ETS1 MFI (B).

(C and D) Layered summary plots of ETS1 MFI (red and left y axis) and Tfh cell frequencies (blue and right y axis) under TGF-β titrated Tfh cell differentiation conditions (C) and correlation of ETS1 MFIs with frequencies of Tfh cell induction (D).

our scope might not have picked up the pathogenic role of Th17 cells. Second, whereas  $Ets1^{\Delta Foxp3}$  and  $Ets1^{\Delta CD19}$  mice showed no signs of humoral autoimmunity, as measured by autoantibody production,  $Ets1^{\Delta Foxp3}$  mice developed spontaneous activation of T cells, and  $Ets1^{\Delta CD19}$  mice had elevated serum IgM concentrations, as previously described (John et al., 2008; Mouly et al., 2010). Thus, dysregulation of Ets1 in Treg and B cells might generate an environment more favorable for humoral autoimmunity, and their synergistic effects must be addressed in the future. Nevertheless, it seems that the cell-intrinsic loss of Ets1 in effector T cells is key for the initiation of autoantibody production in  $Ets1^{-/-}$  mice.

Tfh cell subsets were first described in humans and received attention as autoimmune patients displayed dysregulation of their ratios. Subsequently, the role of Tfh1 cells in augmenting anti-viral responses has been illustrated in mice (Weinstein et al., 2018). However, Tfh17 and Tfh2 cells are yet to be described in murine systems. There are, however, a plethora of reports regarding IL-4-producing Tfh cells in the context of B cell activation, IgE class switching, anti-helminth immunity, and asthma, and these cells could be considered murine versions of Tfh2 cells (Kobayashi et al., 2016; Meli et al., 2017; Reinhardt et al., 2009; Weinstein et al., 2016; Yusuf et al., 2010). Nevertheless, in contrast to human Tfh2 cells, the IL-4+ Tfh cells examined in these reports do not express GATA-3. Here, we report IL-4+ Tfh2 cells that were GATA-3+Bcl6+. GATA3+Bcl6+ Tfh2 cells acted like conventional Tfh cells in that they could induce GC reactions. This brings up the question of whether previously reported IL-4<sup>+</sup> Tfh cells and the currently reported GATA-3+Bcl6+Tfh2 cells are the same or whether they have their differences. An additional question that needs to be addressed is how GATA-3 is expressed in the presence of Bcl6, GATA-3's transcriptional repressor (Kusam et al., 2003). One explanation we identified is that pSTAT6 and Bcl6 share binding motifs at the Gata3 locus, and the enhanced pSTAT6 signaling in Ets1-deficient Tfh cells could outcompete Bcl6 for binding the Gata3 locus. However, this hypothesis requires further examination. Moreover, we have demonstrated that IL-4 is the key pathogenic cytokine in  $\it Ets1^{\Delta CD4}$  mice given that IL-4 neutralization decreased symptoms of autoimmunity. In relation to this, we would like to address the clinical trials of blocking ICOSL signaling for treating SLE. This strategy targets

total Tfh cells, which could compromise the immune system because Tfh1 cells are important for anti-viral responses (Bentebibel et al., 2013). Therefore, establishing strategies for manipulating Tfh cells in a subset-specific manner might prove important. In this light, IL-4 is a promising target for specific inhibition of Tfh2 cells. However, to use IL-4 as a target for immunotherapy, further studies will be needed to determine whether IL-4 acts on B cells, CD4 T cells, or both by generating mixed-bone-marrow chimeras in which IL-4R (or STAT6) is selectively absent in B or T cells.

As a side note, although the increase in Tfh2 cells was the most notable, we also saw increases in IL-17<sup>+</sup>Tfh17, IFN- $\gamma$ <sup>+</sup> Th1, and IFN- $\gamma$ <sup>+</sup> Tfh1 cells in *Ets1*<sup> $\Delta$ CD4</sup> mice. Tfh17 cells are increased in autoimmune diseases such as rheumatoid arthritis and Sjögren's syndrome (Morita et al., 2011), whereas Th1 cells are linked to skin injury, and IFN- $\gamma$  is known to induce IgG2 isotype switching in B cells. Therefore, the role of Ets1 in Th1, Tfh1, and Tfh17 cell biology and their subsequent contributions to autoimmunity might be an important issue to pursue in the future.

A key role of Tfh2 cells is the induction of IgE, which is the effector arm in type 2 humoral immunity (Meli et al., 2017; Wu and Scheerens, 2014; Wu and Zarrin, 2014). IgE is also implicated in autoimmunity; SLE patients have high serum titers of anti-dsDNA IgE, and these positively correlate with SLEDAI scores (Augusto et al., 2018; Dema et al., 2014). Functionally, self-reactive IgE is thought to activate basophils and pDCs and thus cause them to migrate to lymphoid organs to further activate B cells and T cells (Charles et al., 2010; Henault et al., 2016). This pathway, however, is an upstream mechanism and does not explain the function of IgE deposits found in the skin and kidney. The skin and kidney are the two most common sites of pathology in SLE patients; therefore, understanding the function of IgE deposits will be fundamental to SLE research. On a different note, IgE can be produced through either a GC or an extrafollicular pathway, which determines the affinity and longevity of the humoral response (Wu and Zarrin, 2014). Thus, elucidating markers to identify both pathways and comparing their subsequent disease phenotypes will enable us to better design therapeutics to match individual patients' needs. Along these lines, although we have mainly examined the contribution of the GC pathway to autoimmunity in  $Ets1^{\Delta CD4}$  mice, further studies should analyze the extrafollicular pathway and determine the

<sup>(</sup>E) Histograms of ETS1 expression in active SLE (red), inactive SLE (blue), healthy control individuals (NCs; black), and isotype controls (gray) and a summary graph (right).

<sup>(</sup>F) Summary graph of SLE Disease Activity Index (SLEDAI) scores in ETS1high and ETS1low groups.

<sup>(</sup>G) Correlation analysis of ETS1 MFIs with SLEDAI scores of individual SLE patients.

<sup>(</sup>H) Box-and-whisker plot of ETS1 MFI within Tfh1, Tfh2, and Tfh17 cells. MFI values were normalized to those of CD4+CD45RA+ cells.

<sup>(</sup>I) Summary graph of Tfh2 cell frequencies in ETS1<sup>high</sup> and ETS1<sup>low</sup> groups.

<sup>(</sup>J) Correlation analysis of ETS1 MFIs with Tfh2 cell frequencies in individual SLE patients.

<sup>(</sup>K) Summary graph of frequencies of Tfh2 cells in the indicated groups.

<sup>(</sup>L) Correlation analysis of Tfh2 frequencies with SLEDAI scores.

<sup>(</sup>M) Summary graph of IL-4, IL-5, IL-13, and IL-21 expression within Tfh2 cells in NCs and SLE patients.

<sup>(</sup>N) Correlation analysis of IL-4<sup>+</sup> of Tfh2 cell frequencies with SLEDAI scores.

<sup>(</sup>O–P) Representative flow-cytometric plot of CD20<sup>-</sup>CD38<sup>+</sup> plasmablast (left) with summary graph (right) (O) and summary graph of IgG concentrations in culture supernatants (P) in the indicated groups.

<sup>(</sup>Q) Correlation analysis of Tfh2 cells with α-dsDNA.

Data from flow cytometry and ELISA are representative of at least three independent experiments, and horizontal bars denote mean  $\pm$  SEM. For (B), (D), (E), (G), and (H), a two-tailed unpaired Student's t test was used for statistical analysis: \*p < 0.05, \*\*p < 0.01, \*\*\*p < 0.001, \*\*\*\*p < 0.0001. Goodness-of-fit  $r^2$  values for (C), (F), (and (J)–(L) are indicated: \*p < 0.05, \*\*p < 0.01, \*\*\*\*p < 0.0001. See also Figure S6 and S7.

source of PCs in  $Ets1^{\Delta CD4}$  mice in order to draw a more comprehensive picture of humoral autoimmunity in SLE.

#### **STAR**\*METHODS

Detailed methods are provided in the online version of this paper and include the following:

- KEY RESOURCES TABLE
- CONTACT FOR REAGENT AND RESOURCE SHARING
- EXPERIMENTAL MODEL AND SUBJECT DETAILS
  - Mouse Strains
  - Human Studies
- METHOD DETAILS
  - O Flow cytometric analysis
  - FLISA
  - O Urine Albumin ELISA
  - Immunofluorescence and Histology
  - O T cell B cell co-culture assay
  - Tfr suppression assay
  - O Tem and Tfh help to B cells
  - O Adoptive Cell Transfers and Immunization
  - Western Blot
  - RNA-seq analysis
  - ChIP-seq analysis
  - O ATAC-seg analysis
  - O Gene set enrichment analysis (GSEA)
  - O RNA Isolation, cDNA synthesis, quantitative rt-PCR
  - In vivo IL-4 neutralization
  - O Human peripheral blood mononuclear cells
  - O Human cytokine expression analysis
  - O In vitro differentiation of human Tfh cells
  - O Human Tfh2- Naïve B cell co-culture assay
- QUANTIFICATION AND STATISTICAL ANALYSIS
- DATA AND SOFTWARE AVAILABILITY

#### SUPPLEMENTAL INFORMATION

Supplemental Information includes seven figures and four tables and can be found with this article online at https://doi.org/10.1016/j.immuni.2018.10.012.

#### **ACKNOWLEDGMENTS**

We thank Dr. Meinrad Busslinger for agreeing to provide *Gata3* <sup>GFP</sup> mice and Dr. Maxime Bouchard for providing us with the mice. We also thank Haejin Jung for technical assistance for cell sorting. This work was supported by grants from the Korea Health Technology R&D project funded by the Ministry of Health & Welfare (HI16C0992 to C.-H.S.) and by the Institute for Basic Science (IBS-R005 to S.-H.I.).

#### **AUTHOR CONTRIBUTIONS**

C.J.K. and S.-H.I. designed the studies and wrote the manuscript. C.J.K. performed most of the experiments and analyzed the data. C.G.L. and S.-H.I. participated in data acquisition and provided technical and intellectual support to the project. C.-H.S., J.-Y.J., and C.J.K. participated in recruitment and analysis of SLE patients. S.M.H., H.K., and C.L. participated in experiments. A.G. and C.J.K. performed RNA-seq and ChIP-seq data analysis, and N.S.H., A.G., G.K., and C.J.K. performed ATAC-seq analysis. D.R. provided intellectual sugestions during the course of the study and edited the manuscript along with S.-H.I. S.-H. I. has full access to all data in the study and takes responsibility for the integrity of the data, as well as for the manuscript. All authors have read and approved the final manuscript.

#### **DECLARATION OF INTERESTS**

The authors declare no competing interests.

Received: March 27, 2018 Revised: August 28, 2018 Accepted: October 14, 2018

Published: December 18, 2018; corrected online: December 24, 2018

#### **REFERENCES**

Augusto, J.-F., Truchetet, M.-E., Charles, N., Blanco, P., and Richez, C. (2018). IgE in lupus pathogenesis: friends or foes? Autoimmun. Rev. *17*, 361–365.

Banchereau, J., and Pascual, V. (2006). Type I interferon in systemic lupus erythematosus and other autoimmune diseases. Immunity 25, 383–392.

Bentebibel, S.E., Lopez, S., Obermoser, G., Schmitt, N., Mueller, C., Harrod, C., Flano, E., Mejias, A., Albrecht, R.A., Blankenship, D., et al. (2013). Induction of ICOS+CXCR3+CXCR5+ TH cells correlates with antibody responses to influenza vaccination. Sci. Transl. Med. *5*, 176ra32.

Blanco, P., Ueno, H., and Schmitt, N. (2016). T follicular helper (Tfh) cells in lupus: activation and involvement in SLE pathogenesis. Eur. J. Immunol. *46*, 281–290.

Buenrostro, J.D., Wu, B., Chang, H.Y., and Greenleaf, W.J. (2015). ATAC-seq: a method for assaying chromatin accessibility genome-wide. Curr. Protoc. Mol. Biol. 109, 1–9.

Charles, N., Hardwick, D., Daugas, E., Illei, G.G., and Rivera, J. (2010). Basophils and the T helper 2 environment can promote the development of lupus nephritis. Nat. Med. *16*, 701–707.

Crotty, S. (2011). Follicular helper CD4 T cells (TFH). Annu. Rev. Immunol. 29, 621–663

Crow, M.K. (2014). Type I interferon in the pathogenesis of lupus. J. Immunol. 192. 5459–5468.

Dema, B., Pellefigues, C., Hasni, S., Gault, N., Jiang, C., Ricks, T.K., Bonelli, M.M., Scheffel, J., Sacré, K., Jablonski, M., et al. (2014). Autoreactive IgE is prevalent in systemic lupus erythematosus and is associated with increased disease activity and nephritis. PLoS ONE 9, e90424.

Dörner, T., Jacobi, A.M., and Lipsky, P.E. (2009). B cells in autoimmunity. Arthritis Res. Ther. 11, 247.

Fonseca, V.R., Agua-Doce, A., Maceiras, A.R., Pierson, W., Ribeiro, F., Romão, V.C., Pires, A.R., da Silva, S.L., Fonseca, J.E., Sousa, A.E., et al. (2017). Human blood  $T_{\rm fr}$  cells are indicators of ongoing humoral activity not fully licensed with suppressive function. Sci. Immunol. 2, eaan1487.

Fu, W., Liu, X., Lin, X., Feng, H., Sun, L., Li, S., Chen, H., Tang, H., Lu, L., Jin, W., and Dong, C. (2018). Deficiency in T follicular regulatory cells promotes autoimmunity. J. Exp. Med. *215*, 815–825.

Garrett-Sinha, L.A. (2013). Review of Ets1 structure, function, and roles in immunity. Cell. Mol. Life Sci. 70, 3375–3390.

Grenningloh, R., Kang, B.Y., and Ho, I.C. (2005). Ets-1, a functional cofactor of T-bet, is essential for Th1 inflammatory responses. J. Exp. Med. 201, 615–626.

Henault, J., Riggs, J.M., Karnell, J.L., Liarski, V.M., Li, J., Shirinian, L., Xu, L., Casey, K.A., Smith, M.A., Khatry, D.B., et al. (2016). Self-reactive IgE exacerbates interferon responses associated with autoimmunity. Nat. Immunol. *17*, 196–203.

John, S.A., Clements, J.L., Russell, L.M., and Garrett-Sinha, L.A. (2008). Ets-1 regulates plasma cell differentiation by interfering with the activity of the transcription factor Blimp-1. J. Biol. Chem. 283, 951–962.

Johnston, R.J., Poholek, A.C., DiToro, D., Yusuf, I., Eto, D., Barnett, B., Dent, A.L., Craft, J., and Crotty, S. (2009). Bcl6 and Blimp-1 are reciprocal and antagonistic regulators of T follicular helper cell differentiation. Science *325*, 1006–1010.

Kaul, A., Gordon, C., Crow, M.K., Touma, Z., Urowitz, M.B., van Vollenhoven, R., Ruiz-Irastorza, G., and Hughes, G. (2016). Systemic lupus erythematosus. Nat. Rev. Dis. Primers 2, 16039.

Kim, Y.U., Lim, H., Jung, H.E., Wetsel, R.A., and Chung, Y. (2015). Regulation of autoimmune germinal center reactions in lupus-prone BXD2 mice by follicular helper T cells. PLoS ONE *10*, e0120294.

Kobayashi, T., Iijima, K., Chen, C.-C., Dent, A.L., and Kita, H. (2016). Follicular helper T (Tfh) cells are indispensable for IgE antibody responses to airborne allergens. J. Allergy Clin. Immunol. *137*, AB1.

Kusam, S., Toney, L.M., Sato, H., and Dent, A.L. (2003). Inhibition of Th2 differentiation and GATA-3 expression by BCL-6. J. Immunol. *170*, 2435–2441.

Lattin, J.E., Schroder, K., Su, A.I., Walker, J.R., Zhang, J., Wiltshire, T., Saijo, K., Glass, C.K., Hume, D.A., Kellie, S., and Sweet, M.J. (2008). Expression analysis of G Protein-Coupled Receptors in mouse macrophages. Immunome Res. 4, 5.

Lin, W., Truong, N., Grossman, W.J., Haribhai, D., Williams, C.B., Wang, J., Martín, M.G., and Chatila, T.A. (2005). Allergic dysregulation and hyperimmunoglobulinemia E in Foxp3 mutant mice. J. Allergy Clin. Immunol. *116*, 1106–1115.

Lisnevskaia, L., Murphy, G., and Isenberg, D. (2014). Systemic lupus erythematosus. Lancet 384, 1878–1888.

Locci, M., Wu, J.E., Arumemi, F., Mikulski, Z., Dahlberg, C., Miller, A.T., and Crotty, S. (2016). Activin A programs the differentiation of human TFH cells. Nat. Immunol. *17*. 976–984.

Ma, J., Zhu, C., Ma, B., Tian, J., Baidoo, S.E., Mao, C., Wu, W., Chen, J., Tong, J., Yang, M., et al. (2012). Increased frequency of circulating follicular helper T cells in patients with rheumatoid arthritis. Clin. Dev. Immunol. *2012*, 827480.

Martin, J.C., Baeten, D.L., and Josien, R. (2014). Emerging role of IL-17 and Th17 cells in systemic lupus erythematosus. Clin. Immunol. *154*, 1–12.

Meli, A.P., Fontés, G., Leung Soo, C., and King, I.L. (2017). T follicular helper cell-derived IL-4 is required for IgE production during intestinal helminth infection. J. Immunol. 199, 244–252.

Messi, M., Giacchetto, I., Nagata, K., Lanzavecchia, A., Natoli, G., and Sallusto, F. (2003). Memory and flexibility of cytokine gene expression as separable properties of human T(H)1 and T(H)2 lymphocytes. Nat. Immunol. 4, 78–86.

Mok, M.Y., and Shoenfeld, Y. (2016). Recent advances and current state of immunotherapy in systemic lupus erythematosus. Expert Opin. Biol. Ther. 16, 927–939.

Morita, R., Schmitt, N., Bentebibel, S.E., Ranganathan, R., Bourdery, L., Zurawski, G., Foucat, E., Dullaers, M., Oh, S., Sabzghabaei, N., et al. (2011). Human blood CXCR5(+)CD4(+) T cells are counterparts of T follicular cells and contain specific subsets that differentially support antibody secretion. Immunity 34, 108–121.

Mouly, E., Chemin, K., Nguyen, H.V., Chopin, M., Mesnard, L., Leite-de-Moraes, M., Burlen-defranoux, O., Bandeira, A., and Bories, J.C. (2010). The Ets-1 transcription factor controls the development and function of natural regulatory T cells. J. Exp. Med. 207, 2113–2125.

Park, S., Lee, S., Lee, C.G., Park, G.Y., Hong, H., Lee, J.S., Kim, Y.M., Lee, S.B., Hwang, D., Choi, Y.S., et al. (2017). Capicua deficiency induces autoimmunity and promotes follicular helper T cell differentiation via derepression of ETV5. Nat. Commun. *8*, 16037.

Ramírez, F., Ryan, D.P., Grüning, B., Bhardwaj, V., Kilpert, F., Richter, A.S., Heyne, S., Dündar, F., and Manke, T. (2016). deepTools2: a next generation web server for deep-sequencing data analysis. Nucleic Acids Res. *44* (W1), W160–W165.

Reichlin, M., and Wolfson-Reichlin, M. (2003). Correlations of anti-dsDNA and anti-ribosomal P autoantibodies with lupus nephritis. Clin. Immunol. 108 69–72

Reinhardt, R.L., Liang, H.-E., and Locksley, R.M. (2009). Cytokine-secreting follicular T cells shape the antibody repertoire. Nat. Immunol. 10, 385–393.

Richards, H.B., Satoh, M., Jennette, J.C., Croker, B.P., Yoshida, H., and Reeves, W.H. (2001). Interferon-gamma is required for lupus nephritis in mice treated with the hydrocarbon oil pristane. Kidney Int. *60*, 2173–2180.

Sage, P.T., and Sharpe, A.H. (2015). In vitro assay to sensitively measure T(FR) suppressive capacity and T(FH) stimulation of B cell responses. Methods Mol. Biol. 1291, 151–160.

Samstein, R.M., Arvey, A., Josefowicz, S.Z., Peng, X., Reynolds, A., Sandstrom, R., Neph, S., Sabo, P., Kim, J.M., Liao, W., et al. (2012). Foxp3 exploits a pre-existent enhancer landscape for regulatory T cell lineage specification. Cell *151*, 153–166.

Schmidl, C., Hansmann, L., Lassmann, T., Balwierz, P.J., Kawaji, H., Itoh, M., Kawai, J., Nagao-Sato, S., Suzuki, H., Andreesen, R., et al.; FANTOM consortium (2014). The enhancer and promoter landscape of human regulatory and conventional T-cell subpopulations. Blood *123*, e68–e78.

Schmitt, N., Liu, Y., Bentebibel, S.E., Munagala, I., Bourdery, L., Venuprasad, K., Banchereau, J., and Ueno, H. (2014). The cytokine TGF- $\beta$  co-opts signaling via STAT3-STAT4 to promote the differentiation of human TFH cells. Nat. Immunol. *15*, 856–865.

Seder, R.A., Paul, W.E., Davis, M.M., and Fazekas de St Groth, B. (1992). The presence of interleukin 4 during in vitro priming determines the lymphokine-producing potential of CD4+ T cells from T cell receptor transgenic mice. J. Exp. Med. 176, 1091–1098.

Subramanian, A., Tamayo, P., Mootha, V.K., Mukherjee, S., Ebert, B.L., Gillette, M.A., Paulovich, A., Pomeroy, S.L., Golub, T.R., Lander, E.S., and Mesirov, J.P. (2005). Gene set enrichment analysis: a knowledge-based approach for interpreting genome-wide expression profiles. Proc. Natl. Acad. Sci. USA 102, 15545–15550.

Sun, C., Molineros, J.E., Looger, L.L., Zhou, X.J., Kim, K., Okada, Y., Ma, J., Qi, Y.Y., Kim-Howard, X., Motghare, P., et al. (2016). High-density genotyping of immune-related loci identifies new SLE risk variants in individuals with Asian ancestry. Nat. Genet. 48, 323–330.

Trapnell, C., Hendrickson, D.G., Sauvageau, M., Goff, L., Rinn, J.L., and Pachter, L. (2013). Differential analysis of gene regulation at transcript resolution with RNA-seq. Nat. Biotechnol. *31*, 46–53.

Tsao, H.W., Tai, T.S., Tseng, W., Chang, H.H., Grenningloh, R., Miaw, S.C., and Ho, I.C. (2013). Ets-1 facilitates nuclear entry of NFAT proteins and their recruitment to the IL-2 promoter. Proc. Natl. Acad. Sci. USA *110*, 15776–15781.

Vinuesa, C.G., Linterman, M.A., Yu, D., and MacLennan, I.C. (2016). Follicular helper T cells. Annu. Rev. Immunol. *34*, 335–368.

Wang, D., John, S.A., Clements, J.L., Percy, D.H., Barton, K.P., and Garrett-Sinha, L.A. (2005). Ets-1 deficiency leads to altered B cell differentiation, hyperresponsiveness to TLR9 and autoimmune disease. Int. Immunol. *17*, 1179–1191.

Weinstein, J.S., Herman, E.I., Lainez, B., Licona-Limón, P., Esplugues, E., Flavell, R., and Craft, J. (2016). TFH cells progressively differentiate to regulate the germinal center response. Nat. Immunol. *17*, 1197–1205.

Weinstein, J.S., Laidlaw, B.J., Lu, Y., Wang, J.K., Schulz, V.P., Li, N., Herman, E.I., Kaech, S.M., Gallagher, P.G., and Craft, J. (2018). STAT4 and T-bet control follicular helper T cell development in viral infections. J. Exp. Med. *215*, 337–355.

Wu, L.C., and Scheerens, H. (2014). Targeting IgE production in mice and humans. Curr. Opin. Immunol. 31, 8–15.

Wu, L.C., and Zarrin, A.A. (2014). The production and regulation of IgE by the immune system. Nat. Rev. Immunol. *14*, 247–259.

Wu, C., Jin, X., Tsueng, G., Afrasiabi, C., and Su, A.I. (2016). BioGPS: building your own mash-up of gene annotations and expression profiles. Nucleic Acids Res. 44 (D1), D313–D316.

Yang, W., Shen, N., Ye, D.Q., Liu, Q., Zhang, Y., Qian, X.X., Hirankarn, N., Ying, D., Pan, H.F., Mok, C.C., et al.; Asian Lupus Genetics Consortium (2010). Genome-wide association study in Asian populations identifies variants in ETS1 and WDFY4 associated with systemic lupus erythematosus. PLoS Genet. 6, e1000841.

Yusuf, I., Kageyama, R., Monticelli, L., Johnston, R.J., Ditoro, D., Hansen, K., Barnett, B., and Crotty, S. (2010). Germinal center T follicular helper cell IL-4 production is dependent on signaling lymphocytic activation molecule receptor (CD150). J. Immunol 185, 190–202.

Zhu, J., Yamane, H., and Paul, W.E. (2010). Differentiation of effector CD4 T cell populations (\*). Annu. Rev. Immunol. 28, 445–489.

# **STAR**\***METHODS**

# **KEY RESOURCES TABLE**

REAGENT or RESOURCE	SOURCE	IDENTIFIER
Antibodies		
Anti-mouse CD4 (GK1.5)-BUV395	BD Biosciences	Cat# 563790; RRID: AB_2734761
Anti-mouse CD8a antibody (53-6.7)-PerCP/Cy5.5	Biolegend	Cat# 100733; RRID: AB_2075239
Anti-mouse/human CD45R/B220 (RA3-6B2)-FITC	Biolegend	Cat# 103206; RRID: AB_312991
Anti-mouse CD19 (6D5)-BV421	Biolegend	Cat# 115538; RRID: AB_11203527
Anti-mouse CD11c (N418)-BV421	Biolegend	Cat# 117330; RRID: AB_11219593
Anti-mouse CD86 (GL-1)-BV605	Biolegend	Cat# 105037; RRID: AB_11204429
Anti-mouse CD45.2 (104)-FITC	Biolegend	Cat# 109806; RRID: AB_313443
Anti-mouse/human CD44 (IM7)-FITC	Biolegend	Cat# 103006; RRID: AB_312957
Anti-mouse CD62L (MEL-14)-APC	Biolegend	Cat# 104411; RRID: AB_313098
Anti-mouse CD69 (H1.2F3)-FITC	Biolegend	Cat# 104506; RRID: AB_313109
Anti-mouse CD138 (281-2)-PE/Cy7	Biolegend	Cat# 142514; RRID: AB_2562198
Anti-mouse CXCR5 (2G8)-Biotin	BD Biosciences	Cat# 551960; RRID: AB_394301
Anti-mouse CXCR5 (L138D7)-BV421	Biolegend	Cat# 145512; RRID: AB_2562128
Anti-mouse CD90.1 (OX-7)-Alexa Fluor 488	Biolegend	Cat# 202505; RRID: AB_492883
Anti-mouse ICOS (ISA-3)-PerCP-eFluor 710	Thermo Fisher Scientific	Cat# 46-9948-41; RRID: AB_10855043
Anti-mouse PD-1 (29.F.1A12)-PE	Biolegend	Cat# 135206; RRID: AB_1877231
Anti-mouse CD95 (SA367H8)-PE	Biolegend	Cat# 152608; RRID: AB_2632902
Anti-mouse GL7 (GL-7)-eFluor 660	Thermo Fisher Scientific	Cat# 50-5902-82; RRID: AB_2574252
Anti-mouse CXCR3 (CXCR3-173)-PE	Biolegend	Cat# 126506; RRID: AB_1027650
Anti-mouse CCR6 (140706)-BV786	BD Biosciences	Cat# 740840; RRID: AB_2740494
Anti-mouse GATA3 (16E10A23)-APC	Biolegend	Cat# 653806; RRID: AB_2562725
Anti-mouse GATA3 (TWAJ)-eFluor 660	Thermo Fisher Scientific	Cat# 50-9966-42; RRID: AB_10596660
Anti-mouse T-bet (4B10)-PE/Cy7	Biolegend	Cat# 644824; RRID: AB_2561761
Anti-mouse RORγt (AFKJS-9)-PE	Thermo Fisher Scientific	Cat# 12-6988-82; RRID: AB_1834470
Anti-mouse Bcl-6 (7D1)-PE/Cy7	Biolegend	Cat# 358512; RRID: AB_2566196
Anti-mouse Ki-67 (SolA15)-PerCP-eFluor 710	Thermo Fisher Scientific	Cat# 46-5698-82; RRID: AB_1104098
Anti-mouse Foxp3 (FJK-16 s)-FITC	Thermo Fisher Scientific	Cat# 11-5773-82; RRID: AB_465243
Anti-mouse Foxp3 (FJK-16 s)-PE/Cy7	Thermo Fisher Scientific	Cat# 25-5773-82; RRID: AB_891552
Anti-mouse IL4 (11B11)-APC	Biolegend	Cat# 504106; RRID: AB_315320
Anti-mouse IL10 (JES5-16E3)-BV421	Biolegend	Cat# 505022; RRID: AB_2563240
Anti-mouse IL17A (TC11-18H10.1)-PE/Cy7	Biolegend	Cat# 506922; RRID: AB_2125010
Anti-mouse IL21 (FFA21)-PE	Thermo Fisher Scientific	Cat# 12-7211-80; RRID: AB_1834468
Anti-mouse IFN-γ (XMG1.2)-FITC	Thermo Fisher Scientific	Cat# 11-7311-81; RRID: AB_465411
Anti-mouse IgG (R37120)-Alexa Fluor 488	Thermo Fisher Scientific	Cat# R37120; RRID: AB_2556548
Anti-mouse CD3 (17A2)	Biolegend	Cat# 100202; RRID: AB_312659
Anti-rat IgG (Polyclonal)-Alexa Fluor 568	Thermo Fisher Scientific	Cat# A-11077; RRID: AB_2534121
Anti-mouse GL7 (GL-7)-Biotin	Thermo Fisher Scientific	Cat# 13-5902-81; RRID: AB_823152
Streptavidin-Alexa Fluor 647	Thermo Fisher Scientific	Cat# S-21374; RRID: AB_2336066
Anti-mouse IgD ()-Alexa Fluor 488	Biolegend	Cat# 405718; RRID: AB_10730619
Anti-mouse IgM (Polyclonal)-Functional Grade	Thermo Fisher Scientific	Cat# 16-5092-85; RRID: AB_2573088
Anti-mouse CD3ε (145-2C11)	BioXcell	Cat# BE0001-1; RRID: AB_1107634
Anti-human CD4 (RPA-T4)-BUV395	BD Biosciences	Cat# 564724; RRID: AB_2738917
Anti-human CD3 (SK7)-BV510	Biolegend	Cat# 344828; RRID: AB_2563704
Anti-human CD45RA (HI100)-FITC	Biolegend	Cat# 304106; RRID: AB_314410
Anti-human CXCR5 (J252D4)-APC	Biolegend	Cat# 356908; RRID: AB_2561817
	-	

(Continued on next page)

Continued		
REAGENT or RESOURCE	SOURCE	IDENTIFIER
Anti-human CXCR3 (G025H7)-PE	Biolegend	Cat# 353706; RRID: AB_10962912
Anti-human CCR6 (11A9)-BV786	BD Biosciences	Cat# 563704; RRID: AB_2738381
Anti-human PD-1 (EH12.2H7)-PE/Cy7	Biolegend	Cat# 329906; RRID: AB_94048
nti-human ICOS (C398.4A)-FITC	Biolegend	Cat# 313506; RRID: AB_416330
Anti-mouse Ig, Human ads-UNLB	SouthernBiotech	Cat# 1010-01
Anti-mouse IgG, Human ads-HRP	SouthernBiotech	Cat# 1030-05
Anti-mouse IgG1, Human ads-HRP	SouthernBiotech	Cat# 1070-05
Anti-mouse IgG2b, Human ads-HRP	SouthernBiotech	Cat# 1090-05
Anti-mouse IgG2c, Human ads-HRP	SouthernBiotech	Cat# 1079-05
Anti-mouse IgG3, Human ads-HRP	SouthernBiotech	Cat# 1100-05
Anti-mouse IgA-HRP	SouthernBiotech	Cat# 1040-05
Anti-mouse IgE-UNLB	SouthernBiotech	Cat# 1110-01
Anti-mouse IgE-HRP	SouthernBiotech	Cat# 1130-05
Anti-mouse ETS-1 (D808A)	Cell Signaling Technology	Cat# 14069
Anti-mouse beta Actin (mAbcam 8226)	Abcam	Cat# ab8226; RRID: AB_306371
Anti-rabbit IgG (polyclonal)-HRP	AbClon	Cat# AbC-5003
Anti-mouse IgG (polyclonal)-HRP	AbClon	Cat# AbC-5001
Anti-Mouse IgG1-UNLB	Southern Biotech	Cat# 1071-01
Anti-Mouse IgG2b-UNLB	Southern Biotech	Cat# 1091-01
Anti-Mouse IgG2c-UNLB	Southern Biotech	Cat# 1078-01
Anti-Mouse IgG3-UNLB	Southern Biotech	Cat# 1191-01
Anti-Mouse IgE-UNLB	Southern Biotech	Cat# 1110-01
Anti-Mouse Icos PE-Cy7	Biolegend	Cat# 313519; RRID: AB_10641839
Anti-Mouse Ox40 BV711	Biolegend	Cat# 119421; RRID: AB_2687176
Anti-Mouse CD40L APC	Biolegend	Cat# 106510; RRID: AB_2561561
Anti-Human IL5	Biolegend	Cat# 504306; RRID: AB_315330
Anti-Human IL13 PE-Cy7	Biolegend	Cat# 501914, RRID: AB_2616746
Anti-Human CD127 PE-Cy7	Biolegend	Cat# 351320; RRID: AB_10897098
Anti-Human CD25 APC	Biolegend	Cat# 356110; RRID: AB_2561977
Anti-Human Foxp3 Alexa Fluor 488	Biolegend	Cat# 320212; RRID: AB_430887
Anti-Human CD27 BV421	Biolegend	Cat# 356418; RRID: AB_2562599
Anti-Human CD38 PE	Biolegend	Cat# 356604; RRID: AB_2561900
Anti-Human CXCR5 PerCP/Cy5.5	Biolegend	Cat# 356910; RRID: AB_2561819
Anti-Human CD19 Alexa Fluor 488	Biolegend	Cat# 363038; RRID: AB_2728355
nVivoMab anti-mouse IL-4 antibody	BioXcell	Cat# BE0045; RRID: AB_1107707
nVivoMab rat IgG1 isotype control (anti-HRP) antibody	BioXcell	Cat# BE0088; RRID: AB_1107775
Chemicals, Peptides, and Recombinant Proteins		
Dynabeads human T-Activator CD3/CD28	Thermo Fisher Scientific	Cat# 11131D
Recombinant Human IL-12	Peprotech	Cat# 200-06
DAPI	Sigma Aldrich	Cat# D9542
Critical Commercial Assays		
Active Caspase-3 PE apoptosis kit	BD Biosciences	Cat# 550914; RRID: AB_393957
Foxp3 Transcription Factor Staining Buffer Kit	Thermo Fisher Scientific	Cat# A25866A
EasySep Mouse Naive CD4+ T cell Isolation Kit	STEMCELL	Cat# 19765
Naive CD4+ T cell Isolation Kit	Miltenyi	Cat# 130-094-131
ymphoprep	STEMCELL	Cat# 07801

(Continued on next page)

Continued		
REAGENT or RESOURCE	SOURCE	IDENTIFIER
Mouse Albumin ELISA Kit	BETHYL Lab	Cat# E99-134
Mouse IgE ELISA MAX Standard	Biolegend	Cat# 432402
Human IgG ELISA development kit (ALP)	Mabtech	Cat# 3850-1AD-6
Human IgE ELISA development kit (ALP)	Mabtech	Cat# 3810-1H-6
Cell Stimulation Cocktail (plus protein transport nhibitors)	eBioscience/Invitrogen	Cat# 00-4975-03
Deposited Data		
ChIP-seq Human ETS1_Tconv	Schmidl et al., 2014	GEO: GSM1056931
ChIP-seq Mouse Ets1_CD4	Samstein et al., 2012	GEO: GSM999187
RNA-seg WT Non-TFH rep 1	This Study	GEO: GSM3003895
RNA-seg WT Non-TFH rep 2	This Study	GEO: GSM3003896
RNA-seq WT Non-TFH rep 3	This Study	GEO: GSM3003897
RNA-seq WT TFH rep 1	This Study	GEO: GSM3003901
RNA-seq WT TFH rep 2	This Study	GEO: GSM3003902
RNA-seq WT TFH rep 3	This Study	GEO: GSM3003903
RNA-seq Ets1 KO Non-TFH rep 1	This Study	GEO: GSM3003898
RNA-seq Ets1 KO Non-TFH rep 2	This Study	GEO: GSM3003899
RNA-seq Ets1 KO T Non-TFH rep 3	This Study  This Study	GEO: GSM3003990
RNA-seq Ets1 KO TFH rep 1	•	GEO: GSM3003904
·	This Study This Study	GEO: GSM3003904 GEO: GSM3003905
RNA-seq Ets1 KO TFH rep 2 RNA-seq Ets1 KO TFH rep 3	This Study	GEO: GSM3003906
·	·	GEO: GSM3003908
ATAC-seq WT-TN	This Study	
ATAC-seq KO-TN	This Study	GEO: GSM3003893
ATAC-seq WT-TFH	This Study	GEO: GSM3003894
ATAC-seq KO-TFH	This Study	GEO: GSM3038016
Experimental Models: Organisms/Strains		IAV 000004
Mouse: C57BL/6	Jackson Laboratory	JAX: 000664
Mouse: B6.SJL-Ptprca Pepcb/BoyJ	Jackson Laboratory	JAX: 002014
Mouse: B6.Cg-Tg(TcraTcrb)425Cbn/J	Jackson Laboratory	JAX: 004194
Mouse: Tg(Cd4-cre)1Cwi/BfluJ	Jackson Laboratory	JAX: 017336
Mouse: B6.129P2(C)-Cd19tm1(cre)Cgn/J	Jackson Laboratory	JAX: 006785
Mouse: B6.Cg-Tg(ltgax-cre)1-1Reiz/J	Jackson Laboratory	JAX: 008068
Mouse: B6.129S7-Rag1 <sup>tm1Mom</sup> /J	Jackson Laboratory	JAX: 002216
Mouse: Ets1 -/-	Dr. I-Cheng Ho	N/A
Mouse: Ets1 <sup>flox/flox</sup> (Ets1 <sup>flox</sup> )	This Study	N/A
Mouse: CD4-cre Ets1 <sup>flox/flox</sup> (Ets1 <sup>ΔCD4</sup> )	This Study	N/A
Mouse: CD19-cre Ets1 <sup>flox/flox</sup> (Ets1 <sup>ΔCD19</sup> )	This Study	N/A
Mouse: CD11c-cre Ets1 <sup>flox/flox</sup> (Ets1 <sup>ΔCD11c</sup> )	This Study	N/A
Mouse: GATA-3 GFP	Dr. Meinrad Busslinger	N/A
Mouse: B6.129(Cg)-Foxp3tm4(YFP/icre)Ayr/J	Jackson Laboratory	JAX: 016959
Software and Algorithms		
lowjo v.10.2	Tree Star	RRID: SCR_008520
Graphpad Prism 7	Graphpad	RRID: SCR_002798
MORPHEUS	Broadinstitute	RRID: SCR_014975
astQC v0.11.7	OMICtools	RRID: SCR_014583
ГорНat v2.1.1	OMICtools	RRID: SCR_013035
Cufflinks v2.2.1	Cole-Trapnell-lab	RRID: SCR_014597
Cuffmerge v1.0.0		RRID: SCR_015688

(Continued on next page)

Continued				
REAGENT or RESOURCE	SOURCE	IDENTIFIER		
Cuffdiff v2.2.1	OMICtools	RRID: SCR_001647		
Cutadapt v1.9.1	OMICtools	RRID: SCR_011841		
SAMtools v1.2	Genetic Analysis Software	RRID: SCR_002105		
Bowtie2 v2.2.6	OMICtools	RRID: SCR_005476		
Bedtools v2.26	OMICtools	RRID: SCR_006646		
MACSv2	OMICtools	RRID: SCR_013291		
GSEA	OMICtools	RRID: SCR_003199		
Integrative Genomics Viewer	OMICtools	RRID: SCR_011793		
ImageJ	NIH	RRID: SCR_003070		
UCSC Genome Browser	Science Exchanger	RRID: SCR_012479		
Primers				
Bc/6 F: CTT ACC ATT GTG AGA AGT GTA ACC Bc/6 R: CAT CCT TTG GGT AGA TTC TGA G	PrimerBank	N/A		
Batf F: CTG GCA AAC AGG ACT CAT CTG Batf R: GGG TGT CGG CTT TCT GTG TC	PrimerBank	N/A		
Etv5 F: TCA GTC TGA TAA CTT GGT GCT TC Etv5 R: GGC TTC CTA TCG TAG GCA CAA	PrimerBank	N/A		
Egr2 F: GCC AAG GCC GTA GAC AAA ATC Egr2 R: CCA CTC CGT TCA TCT GGT CA	PrimerBank	N/A		
Gata3 F: CTC GGC CAT TCG TAC ATG GAA Gata3 R: GGA TAC CTC TGC ACC GTA GC	PrimerBank	N/A		
II4 F: CAA CGA AGA ACA CCA CAG AG II4 R: GGA CTT GGA CTC ATT CAT GG	PrimerBank	N/A		
II7r F: GCG GAC GAT CAC TCC TTC TG II7r R: AGC CCC ACA TAT TTG AAA TTC CA	PrimerBank	N/A		

# **CONTACT FOR REAGENT AND RESOURCE SHARING**

Further information and requests for resources and reagents should be directed to and will be fulfilled by the Lead Contact, Sin-Hyeog Im (iimsh@postech.ac.kr).

## **EXPERIMENTAL MODEL AND SUBJECT DETAILS**

C57BL/6, CD45.1 B6, OT-II TCR Tg, CD4-cre, CD19-cre, Rag1-/-, CD11c-cre, and Foxp3-cre mice were originally obtained from Jackson Laboratory. Ets1<sup>-/-</sup> mice carrying a germline deletion of Ets1 were previously described (Grenningloh et al., 2005), and kindly provided by Dr. I-Cheng Ho (Harvard Medical School, MA, USA). Gata3 GFP mice were kindly provided by Dr. Meinrad Busslinger (Research Institute of Molecular Pathology (IMP), Vienna Biocenter (VBC), Austria). Ets1flox mice were generated by Toolgen and Macrogen (Seoul, Korea). In brief, RNA-guided endonucleases (RGENs) mediating targeted genome modification was performed against 7<sup>th</sup> exon of *Ets1* which contains part of the DNA binding domain. T cell specific Ets1 deficient mice ( $Ets1^{\Delta CD4}$ ) were generated by breeding  $Ets1^{flox}$  mice to CD4-cre mice;  $Ets1^{\Delta CD19}$ ,  $Ets1^{\Delta CD11c}$ , and  $Ets1^{\Delta Foxp3}$  mice were generated in similar fashion. All mice were maintained in the animal facility of POSTECH Biotech Center in Specific Pathogen Free Condition. Mixtures of male and female mice were used, matched between groups. Mice were sacrificed between the age of 6-8 weeks. In the case of survival curve and skin lesion occurrence, mice were kept till over 40 to less than 60 weeks. All experimental procedures were approved by the POSTECH Institutional Animal Care and Use Committee.

## **Human Studies**

Systemic Lupus Erythematosus (SLE) disease subjects and healthy donors were recruited from the Department of Rheumatology at Ajou University Hospital. Details regarding demographics of subjects are described in Table S2. All studies were reviewed and approved by the Ajou Institutional Review Board (Ajou IRB; approval number, AJIRB-BMR-SMP-17-155). All SLE disease subjects and healthy donors were recruited with informed consents after IRB approval

## **METHOD DETAILS**

#### Flow cytometric analysis

For mice samples, single cell suspensions from peripheral lymph nodes, mesenteric lymph nodes and spleen were prepared and stained with Fixable Viability Dye (Invitrogen) to label dead cells and stained with fluorochrome-conjugated antibodies. For surface staining, cells were washed with PBS and stained with the following antibodies (From Biolegend, BD PharMingen, and eBioscience/ Invitrogen): anti-CD4 (GK1.5 and RM4-5), anti-CD8 (53-6.7), anti-B220 (RA3-6B2), anti-CD19 (6D5), anti-CD11c (N418), anti-CD86 (GL-1), anti-CD45.2 (104), anti-CD44 (IM7), anti-CD62L (MEL-14), anti-CD69 (H1.2F3), anti-CD138 (281-2), anti-CXCR5 (2G8 and L138D7), anti-CD90.1 (OX-7), anti-ICOS (ISA-3), anti-PD-1 (19F.1A12), anti-CD95 (SA367H8), anti-GL7 (GL7), anti-CXCR3 (CXCR3-173), anti-CCR6 (140706), anti-Icos (C398.4A), anti-Ox40L(OX-86), anti-CD40L (MR1). For intracellular transcription factor staining, cells were fixed with eBioscience/Invitrogen Foxp3 Fix/Perm Buffer washed with eBioscience/Invitrogen Perm Buffer and stained with the following antibodies: anti-GATA3 (16E10A23 and TWAJ), anti-T-bet (4B10), anti-RORyt (AFKJS-9), anti-Foxp3 (FJK-16 s), anti-Bcl6 (7D1), anti-Ki67 (SolA15). Two methods were used for intracellular cytokine staining, (1) Cells were stimulated by PMA and ionomycin in the presence of Golgi-Plug (555029, BD) or Golgi-Stop (554724, BD) for 4 hr (2) Cells were stimulated with Cell Stimulation Cocktail plus protein inhibitors (00-4975-03, eBioscience/Invitrogen). After stimulation, cells were washed and surface molecules were stained. Cells were then fixed with eBioscience/Invitrogen Intracellular (IC) Fixation Buffer, washed with Perm Buffer and stained with the following antibodies: anti-IL-4 (11B11), anti-IL-10 (JES5-16E3), anti-IL-17A (TC11-18H10.1), anti-IL-21 (FFA21), anti-IFNγ (XMG1.2). For detection of cellular apoptosis, FITC Annexin V Apoptosis Detection Kit I (BD PharMingen) and PE Active Caspase-3 Apoptosis Kit (BD PharMingen) were used, following the manufacturer's instructions. Cell acquisition was performed on LSR Fortessa (BD Bioscience) and data was analyzed using FlowJo software suite (Tree Star).

#### **ELISA**

Levels of IgG1, IgG2b, IgG2c, IgG3 and IgA were detected from serum of indicated mice. 96 well ELISA plates were coated with antimouse Ig (1010-01, Southern Biotech) or anti-mouse IgE (1110-01, Southern Biotech) and blocked with 1% BSA 0.1% PBST. Diluted serum samples along with reference serum (RS10-101, Bethyl) were loaded, and anti-mouse IgG1-HRP (1070-05, Southern Biotech), anti-mouse IgG2b-HRP (1090-05, Southern Biotech), anti-mouse IgG2c-HRP (1079-05, Southern Biotech), anti-mouse IgG3-HRP (1100-05, Southern Biotech), anti-mouse IgE-HRP (1130-05, Southern Biotech), and anti-mouse IgA-HRP (1040-05, Southern Biotech) secondary antibodies added. The bound enzymes were developed by adding TMB solution (7855927, Invitrogen) and stopped by adding 1M  $H_2SO_4$ . Plates were read at 450 nm and the immunoglobulin concentration's calculated according to the standard curve generated by reference serum. For detection of serum anti-dsDNA IgG and IgE, 96 well ELISA plates were coated with 0.01% Poly-L-Lysine solution (25988-63-0, Sigma) for five minutes at room temperature. Plates were coated with 10ug/mL Calf Thymus DNA (9600-5-D, Trevigen) overnight at 4°C. The next day plates were blocked in 1% BSA 0.1% PBST and diluted serum samples were added. Anti-mouse IgG-HRP (1030-05, Southern Biotech) or anti-mouse IgE-HRP (1130-05, Southern Biotech) secondary antibodies were added and the bound enzymes were developed by adding TMB solution (7855927, Invitrogen) and stopped by adding 1M  $H_2SO_4$ . Plates were read at 450 nm.

#### **Urine Albumin ELISA**

Urine mouse albumin was detected using the Mouse Albumin ELISA kit (Catalogue # E99-134) from Bethyl laboratories according to the manufacturer's instructions.

# Immunofluorescence and Histology

For immunofluorescence and confocal imaging, skin and kidneys were excised and snap-frozen in OCT-compound (Fisher HealthCare). 8 µm sections were cut and fixed in  $-20^{\circ}$ C methanol, rehydrated in PBS and blocked with 5% BSA in 0.1% Tween 20 TBS solution. The sections were stained overnight at  $4^{\circ}$ C in a humid chamber with the following antibodies: anti-mouse IgG Alexa Fluor 488 (Polyclonal, Thermofisher), anti-mouse CD3 (17A2, Biolegend), anti-mouse GL7-biotin (GL7, Thermofisher), anti-mouse IgD Alexa Fluor 488 (11-26c.2a, Biolegend), anti-rat IgG Alexa Fluor 568 (polyclonal, Thermofisher), Streptavidin-Alexa Fluor 647 (Thermofisher) anti-mouse IgG1 (Polyclonal, SouthernBiotech), anti-mouse IgG2b (Polyclonal, SouthernBiotech), anti-mouse IgG2c (Polyclonal, SouthernBiotech), anti-mouse IgG3 (Polyclonal, SouthernBiotech), anti-mouse IgG Alexa Fluor 488 (Thermofisher), anti-mouse C3 (Abcam), anti-rat IgG Alexa Fluor 568 (Thermofisher). Nuclei were stained with DAPI (D9542, Sigma) for 10 min at room temperature. Slides were mounted with Permount mounting medium (SP15-100, Fisher scientific) and dried at room temperature overnight. Images were required using LSM 700 confocal microscope (Carl Zeiss) with a 10x water immersion objective. Images were processed and analyzed using Zen (Carl Zeiss) software and fluorescence intensity was quantified using ImageJ software.

For histology, mice were perfused and kidneys excised and fixed overnight in 4% Paraformaldehyde solution at  $4^{\circ}$ C overnight. Tissues were embedded in paraffin, cut into 5  $\mu$ m sections (Leica RM2245), deparaffinized and dehydrated via sequential addition of xylene, 100% ethanol, and 95% ethanol. The sections were then washed in distilled water and stained with Hematoxylin (HHS3, Sigma) and Eosin (HT110132, Sigma). Sections were imaged using a LEICA DFC420 C light microscope. Glomerulonephritis scoring was done on a scale of 0-4, taking into consideration mesangial expansion, endocapillary proliferation, necrosis, and crescent formation. 100 glomeruli were considered per kidney.

#### T cell - B cell co-culture assay

We followed a modified version of a previously described Tfh-B cell co-culture protocol (Kim et al., 2015).  $CD4^+CXCR5^+PD-1^+$  Tfh cells and  $CD4^+CXCR5^-CD44^+CD62L^-$  Tem cells were sorted using FACs Aria (BD Biosciences) from  $Ets1^{flox}$  and  $Ets1^{\Delta CD4}$  mice according to the gating strategies described above. B cells were sorted from  $Ets1^{\Delta CD4}$  mice as  $B220^+$  cells.  $5x10^4$  CD4 $^+$  T cells and  $7.5x10^4$  B220 $^+$  B cells were cultured together in 96 U-bottomed plates (3799, Corning Costar) in complete medium in the presence of 5  $\mu$ g/mL anti-CD3 (BioXcell) and 1  $\mu$ g/mL anti-IgM (Invitrogen). Supernatants were collected after 6 days of culture, and IgE or IgG were detected using ELISA.

#### Tfr suppression assay

CD4+CXCR5+PD-1+GITR<sup>-</sup> Tfh cells and B220+ B cells were isolated from  $Ets1^{\Delta CD4}$  mice, while CD4+CXCR5+PD-1+GITR+ Tfr cells were isolated from both  $Ets1^{flox}$  (WT Tfr) and  $Ets1^{\Delta CD4}$  mice (KO Tfr) using FACs Aria (BD Biosciences).  $3x10^3$  Tfh cells,  $60x10^3$  B cells, and  $15x10^3$  WT/KO Tfr cells were cultured together, under indicated groups, in complete medium in the presence of  $\alpha$ -CD3/ $\alpha$ -CD28 dynabeads (Invitrogen) at a ratio of 1:1 for a period of 5 days. At the end of the experiment, culture supernatants were collected, and IqG concentrations were determined by ELISA.

#### Tem and Tfh help to B cells

CD4<sup>+</sup>CXCR5<sup>+</sup>PD-1<sup>+</sup>Tfh cells and CD4<sup>+</sup>CXCR5<sup>-</sup>CD44<sup>+</sup>CD62L<sup>-</sup> Tem cells were sorted using FACs Aria (BD Biosciences) from *Ets1*<sup>flox</sup> and *Ets1*<sup>ACD4</sup>. B cells were sorted from *Ets1*<sup>flox</sup> mice as B220<sup>+</sup>GL7<sup>-</sup>IgD<sup>+</sup> cells. 30x10<sup>3</sup> Tem cells or 30x10<sup>3</sup> Tfh cells were cultured with 80x10<sup>3</sup> B cells in complete media in the presence of dynabeads (Invitrogen) at a ratio of 1:1 for 24 hr. At the end of the experiment, expression of GL7 was examined on B cells.

## **Adoptive Cell Transfers and Immunization**

Adoptive transfer experiments have been previously described (Park et al., 2017). Single cell suspensions were prepared from peripheral lymph nodes and spleens of OT-II  $Ets1^{flox}$  or OT-II  $Ets1^{\Delta CD4}$  mice. CD4+ T cells were enriched using EasySep mouse CD4+ T cell isolation kit (19852, STEMCELL) and sorted as FVD-CD4+CD62L+CD44- T naive cells on a FACS Aria cell sorter (BD Biosciences). 1 × 10<sup>6</sup> naive OT-II cells were intravenously injected into CD45.1 B6 recipient mice. The next day recipient mice were immunized with 100  $\mu$ g OVA (A7641, Sigma) in Imject Alum (77161, Thermofisher). 7 days' post immunization mice were analyzed.

For  $Rag1^{-/-}$  transfer experiments, CD19<sup>+</sup>CD138<sup>-</sup> PC depleted B cells, CD4<sup>+</sup>GITR<sup>-</sup>CXCR5<sup>-</sup>CD44<sup>+</sup>CD62L<sup>-</sup> Treg depleted activated T cells, and CD4<sup>+</sup>GITR<sup>-</sup>CXCR5<sup>+</sup>PD-1<sup>+</sup> Tfr depleted Tfh cells were sorted from  $Ets1^{\Delta CD4}$  mice and transferred to  $Rag1^{-/-}$  host via intravenous route. A total of 2 × 10<sup>6</sup> B cells and 2 × 10<sup>5</sup> Tem or Tfh cells were transferred. Mice were analyzed 7 weeks post adoptive transfer of cells.

## **Western Blot**

Tn (CD4+CD44-CD62L-CXCR5-), Tem (CD4+CD44+CD62L-CXCR5-), and Tfn cells (CD4+CXCR5+PD-1+) were sorted from single cell suspensions of B6 mice using FACS Aria. CD4+, CD19+ and CD11c+ cells were enriched from  $Ets1^{flox}$  and  $Ets1^{\Delta CD4}$ ,  $Ets1^{\Delta CD19}$ ,  $Ets1^{\Delta CD11c}$  mice respectively by positive selection using Miltenyi microbeads. 1 × 10<sup>6</sup> cells from each group were lysed using RIPA lysis buffer and separated by SDS-PAGE. Proteins were detected using the following antibodies: Primary, anti-mouse Ets1 (D808A, CST), anti-mouse Actin (8226, Abcam); Secondary, anti-rabbit IgG HRP (AbC-5003, AbClon), anti-mouse IgG HRP (AbC5001, Abclon). Images were taken on a LAS4000.

#### **RNA-seq analysis**

RNA-seq analysis was done following a modified version of previously described protocols (Trapnell et al., 2013). Spleen and lymph nodes were excised from Ets1<sup>flox</sup> and Ets1<sup>ΔCD4</sup> mice and prepared into single cell suspensions. CD4<sup>+</sup> T cells were enriched by MACs microbeads (L3T4, Miltenyi) and FACs sorted into two populations, Tfh (FVD-CD4<sup>+</sup>CXCR5<sup>+</sup>PD-1<sup>+</sup>) and Non-Tfh (FVD-CD4<sup>+</sup>CXCR5<sup>-</sup>PD-1<sup>-</sup>) cells using Aria sorter (BD Biosciences). Three replicates of each group were prepared. RNA were isolated using RNeasy Mini Kit (74106, QIAGEN) according to manufacturer's instruction. Library were prepped using the Illumina Nextera XT DNA Library prep kit and sequencing done on an Illumina NextSeq 500, paired-end 75 cycles. Quality of the sequences was accessed using FastQC v0.11.7 software. RNA-Seq samples were analyzed using TopHat–Cufflinks pipeline. Reads were mapped to the mm10 genome with TopHat v2.1.1. Transcripts were assembled using Cufflinks v2.2.1. Final transcriptome assembly was performed with cuffmerge v1.0.0, and differential expression was identified with cuffdiff v2.2.1.

# **ChIP-seq analysis**

Human Ets1 ChIP-seq (GEO: GSM1056931) and mouse Ets1 ChIP-seq (GEO: GSM999187) analysis done using conventional T cells were acquired online from Cistrome Data Browser (http://cistrome.org). Images of select gene loci were acquired through the ucsc browser. Raw files are available online (GEO codes in parentheses). ChIP-Seq heatmap generation was performed using deptools v2.5.0 environment (Ramírez et al., 2016). Modules involved in the heatmap generation was computeMatrix and plotHeatmap.

## **ATAC-seq analysis**

Cells were prepared in similar fashion as for RNA-seq analysis. The enriched CD4<sup>+</sup>T cells were FACs sorted into two groups, T naive (Tn) (CD4<sup>+</sup>CD62L<sup>+</sup>CXCR5<sup>-</sup>) and Tfh (CD4<sup>+</sup>CXCR5<sup>+</sup>PD-1<sup>+</sup>) cells. Library were prepared using Nextera DNA Sample Prep Kit and Nextera Index Kit. Libraries were sequenced on a HiSeq 2500. IGV browser. Quality control check of the ATAC-Seq data were performed using FastQC v0.11.7 software and Cutadapt v1.9.1 was used to trim sequences. ATAC-seq data was analyzed using customized version of ATAC-seq/DNase-Seq pipeline developed by Kundaje Lab. SAMtools v1.2, sambamba v0.6.5, Bowtie2 v2.2.6, MarkDuplicates v1.126, bedtools 2.26 and MACSv2 were used as components of the pipeline. Mouse genome version mm10 was considered for this purpose. The data analysis operation was performed in Conda3 environment with BigDataScript version v0.99999e and JDK/JRE version > = 1.8. Generated \*.bigwig files from each of the ATAC-Seq experiments were compared using BigwigCompare v2.5.4 & plots were made using IGV browser (https://github.com/kundajelab/atac\_dnase\_pipelines).

## Gene set enrichment analysis (GSEA)

GSEA was performed using the GSEA program provided from the Broad Institute (http://software.broadinstitute.org/gsea/index.jsp). GSEA map generation was performed using the version: GSEA v3.0; Tools used: GSEAPreranked (Subramanian et al., 2005). Gene sets were generated in-house with genes that had a difference of expression of over 1.5 FC Log<sub>2</sub> values in Tfh cells compared to their expression in Non-Tfh cells.

# RNA Isolation, cDNA synthesis, quantitative rt-PCR

Spleen and lymph nodes were excised from *Ets1*<sup>flox</sup> and *Ets1*<sup>ΔCD4</sup> mice and prepared into single cell suspensions. CD4<sup>+</sup> T cells were enriched by MACs microbeads (L3T4, Miltenyi) and FACs sorted into two populations, CD4<sup>+</sup>CXCR5<sup>-</sup>PD-1<sup>-</sup> non-Tfh cells and CD4<sup>+</sup>CXCR5<sup>-</sup>CD44<sup>-</sup>CD62L<sup>+</sup> Tn cells. Total RNA was extracted using Tri Reagent (MRC) according to manufacturer's instructions. cDNA was synthesized using 500 μg total RNA, oligo(dT) primer (Promega), and Improm-II Reverse Transcriptase (Promega). Rt-PCR was done using SYBR Prmix Ex Taq (Takara). The list of primers used can be found in the Key Resources Table.

#### In vivo IL-4 neutralization

5-week-old  $Ets1^{\Delta CD4}$  mice were injected with 1mg of  $\alpha$ -IL4 neutralizing antibody (BioXcell, BE0045, 11B11,) or with 1mg of  $\alpha$ -HRP isotype controls (BioXcell, BE0088, HRPN), once every day for 14 days via intraperitoneal administration.

# **Human peripheral blood mononuclear cells**

Systemic Lupus Erythematosus (SLE) subjects and healthy donors were recruited from the Department of Rheumatology at Ajou University Hospital. Blood samples were diluted 1:2 in cold PBS and PBMCs isolated by density gradient centrifugation using Lymphoprep (07851, STEMCELL). Isolated PBMCs were stained with Fixable Viability Dye (Invitrogen) to label dead cells and stained with fluorochrome-conjugated antibodies. For surface antigens, cells were first washed with PBS and then stained with the following antibodies (From Biolegend and BD Biosciences): anti-CD4 (RPA-T4), anti-CD3 (SK7), anti-CD45RA (H100), anti-CXCR5 (J252D4), anti-CXCR3 (G025H7), anti-CCR6 (G034E3), anti-PD-1 (EH12.2H7), anti-ICOS (C398.4A), anti-CD19 (SJ25C1), anti-CD20 (2H7), anti-CD38 (HB-7), anti-CD27 (M-T271), anti-IgD (IA6-2), anti-IL-4 (8D4-8), anti-IL5 (TRFK5), anti-IL13 (JES10-5A2), anti-IL21 (3A3-N2.1), anti-FOXP3 (259D), anti-CD25 (M-A251). Cell acquisition was performed on LSR Fortessa (BD Bioscience) and data was analyzed using FlowJo software suite (Tree Star). All studies were reviewed and approved by the Ajou Institutional Review Board (Ajou IRB; approval number, AJIRB-BMR-SMP-17-155). All SLE disease subjects and healthy donors were recruited with informed consents after IRB approval.

## **Human cytokine expression analysis**

PBMCs were isolated using lymphoprep (07851, STEMCELL) and SepMate-50 (86450, STEMCELL) according to manufacturer's instructions. CD4<sup>+</sup> T cells were enriched using Miltenyi human CD4 microbeads (130-045-101, Miltenyi) and cells were stimulated for 12 hr in 24 well plates using Cell stimulation cocktail plus protein transport inhibitors (00-4975-93, eBioscience) in complete medium. After stimulation, cells were washed and stained following the same protocol as for IC staining of murine cells.

## In vitro differentiation of human Tfh cells

Human *in vitro* Tfh differentiation has been previously described (Locci et al., 2016). PBMCs were isolate from blood samples of healthy donors as described above. Tn cells were isolated using Naive CD4<sup>+</sup> T Cell Isolation Kit II, human (Miltenyi Biotec). 8  $\times$  10<sup>4</sup> Tn cells were seeded in 96 U-bottom plates and cultured for 3-5 days. Tfh differentiation conditions were: Dynabeads human T-Activator CD3/CD28 (Thermofisher) a ratio of 1:1 with cell numbers, IL12 (5ng/mL, Peprotech), and human-TGF $\beta$  (1ng/mL). Dynabeads were removed at the end of the experiment, and cells analyzed by flow cytometry.

# Human Tfh2- Naïve B cell co-culture assay

PBMCs were isolated from healthy donors (NC) and SLE patients (SLE) using Lymphoprep (STEMCELL) and SepMate-50 (STEMCELL). FVD-CD19 $^{+}$ CXCR5 $^{+}$ CCR6 $^{-}$ CXCR3 $^{-}$  Tfh2 cells and FVD $^{-}$ CD4 $^{-}$ CD19 $^{+}$ CD27 $^{-}$ IgD $^{+}$  naive B cells were sorted using FACs Aria (BD Bioscience). B cells were pooled together.  $30x10^3$  Tfh2 cells were added to  $50x10^3$  naive B cells in 96 well U-bottom plates. Cells were cultured in complete medium and were given  $\alpha$ -CD3/ $\alpha$ -CD28 dynabeads (Thermofisher) at a ratio of



1:1. At day 5 of culture, cells were analyzed for plasmablast differentiation by flow cytometry (CD19+CD38+lgD-) and lgG was detected from the culture supernatant by ELISA.

# **QUANTIFICATION AND STATISTICAL ANALYSIS**

For statistical analyses, all experiments were performed more than three times. Statistical analyses were performed using the twotailed unpaired Student t test or Goodness of fit values r<sup>2</sup> through Graphpad Prism 7 program. P values below 0.05 were considered significant in the following manner: \*p < 0.05, \*\*p < 0.01, \*\*\*\*p < 0.001, \*\*\*\*p < 0.0001. Within bar graphs, bars represent means while error bars indicate SEM. All inclusion of statistical analyses are indicated in the figure legends of main and supplementary figures.

#### **DATA AND SOFTWARE AVAILABILITY**

The RNA-seq data of Non-Tfh and Tfh cells and ATAC-seq data of Tn and Tfh cells isolated from  $\mathrm{Ets1}^{\mathrm{flox}}$  and  $\mathrm{Ets1}^{\Delta\mathrm{CD4}}$  mice were deposited online under the accession number SuperSeries GEO: GSE110647. RNA-seq data can be found under SubSeries GEO: GSE110595 and ATAC-seq under SubSeries GEO: GSE110594.